

# Smart cooperative control scheme for large-scale wind farms based on a double-layer machine learning framework

Shanghai Yang<sup>a</sup>, Kun Yang<sup>a</sup>, Xiaowei Deng<sup>a,\*</sup>, Jun Yang<sup>a,\*</sup>

<sup>a</sup> Department of Civil Engineering, The University of Hong Kong, Pokfulam, Hong Kong, China

## ARTICLE INFO

### Keywords:

ANN yawed wake model  
Bayesian ML algorithm  
Double-layer ML control framework  
Row-based cooperative control scheme  
Wind distribution  
Wind farm layout

## ABSTRACT

In the real-time cooperative control of large-scale wind farms, the simultaneous achievement of accuracy and efficiency by the optimization framework plays an indispensable role. This paper presents a new double-layer machine learning (ML) framework comprising an Artificial Neural Networks (ANN) yawed wake model and Bayesian ML algorithm to strike a desirable compromise between accuracy and efficiency. Given the control on the iteration number with the scale-up of the wind farm, a novel row-based control scheme is further put forward to improve the optimization rate by reasonably reducing the optimization parameters. Moreover, parametric analysis has been performed considering the wind distribution and layout configuration to explore its applicability compared with the general independent one. The study shows that the novel framework performs favorably in an accurate and efficient power prediction and optimization of the wind farm. The row-based control scheme can further improve the convergence rate of the double-layer optimization framework remarkably at the expense of a slight decrease in optimal power production. The divergence of the wind distribution can dwindle the power gain of the wake steering strategy and weaken the superiority of the row-based cooperative control scheme. The row-based cooperative control scheme is more applicable to the aligned layout than the staggered layout, and this advantage is enhanced with the increase of wind farm scale.

## 1. Introduction

Global power production increasingly relies on renewable energy instead of traditional fossil fuels. According to the Intergovernmental Panel on Climate Change (IPCC) Special Report 15 on global warming, to avoid the global temperatures rising 1.5° over the preindustrial levels, renewable energy needs to substitute coal-based power gradually for the dominant role in the global energy structure, up to 67% by 2050 [1]. The efficient harness of wind energy plays an indispensable role in accomplishing this goal, where the offshore one undoubtedly grows as a promising future trend [2]. Nevertheless, reliable, low-cost offshore wind energy production still faces plenty of challenges in the current level of technology [3], where the fundamental issue lies in the significant power loss because of the complex wake interference. In a large wind farm, the wind turbines are often deployed in close proximity considering finite land and power transmission cost. At the same time, the turbines are generally operated under traditional greedy control, setting the rotor directly perpendicular to the inflow to maximize its own power capture [4,5]. Under such circumstances, large quantities of

the downstream turbines will be inevitably under the full-wake regions of the upwind ones, confronted with the apparent velocity deficit and turbulence increase, thereby impairing their power output and service life. The mainstream approaches to resolving the wake problem can be categorized into two types in accordance with the implementation phase, layout design and yaw control. This paper only focuses on exploring the latter, which steers the wake away from the downwind turbines to mitigate the wake effect as much as possible by adjusting the yaw angle of the upstream turbines.

The present challenges in the yaw control concentrate on the accurate and efficient implementation of the power prediction and optimization, the former relies on the high-fidelity wake characterization of the wind farm, and the latter calls for the rapid convergence of the optimization algorithm. The wake modeling in the engineering practice is generally conducted with the aid of the analytical wake model owing to its simplicity and low computational cost, including some commonly-used unyawed wake models like Jensen model [6], Frandsen model [7], Bastankhah and Porte-Agel model [8], Sun model [9], Dou model [10], and Ishihara & Qian model [11]. It is noteworthy that the above

\* Corresponding authors.

E-mail addresses: [xwdeng@hku.hk](mailto:xwdeng@hku.hk) (X. Deng), [junyang@hku.hk](mailto:junyang@hku.hk) (J. Yang).

<https://doi.org/10.1016/j.enconman.2023.116949>

Received 15 November 2022; Received in revised form 1 March 2023; Accepted 17 March 2023

Available online 11 April 2023

0196-8904/© 2023 Elsevier Ltd. All rights reserved.

analytical yawed wake model performs poorly in accurately predicting the wake flow, which can result from the simplified rotor-flow interaction, the lack of turbulence capture, and some empirical constants without universality. The recent research on the analytical model sets its sights on the yawed wake characterization, and there has emerged some representative yawed wake models, like Bastankhah and Porte-Agel model [12], Shapiro model [13], Lopez model [14], Howland model [1], Gebraad model [15], Dijk model [16], Dou model [17], and Qian & Ishihara model [18]. Nevertheless, besides the intuitive defects of the analytical yawed wake model mentioned above, some new problems arise in these yawed wake models, such as the centrosymmetric simplification of the kidney-shaped wake cross-section. Another common approach to wake modeling is computational fluid dynamics (CFD), a competitive tool for high-resolution simulation of turbine wake targeted at some scientific problems but too computationally expensive for practical use in engineering, mainly including Reynolds-averaged Navier-Stokes (RANS) and Large Eddy Simulation (LES). Given the flaws in wake modeling using the analytical wake model and CFD, the advanced machine learning (ML) technique is recently applied in wake modeling to strive for a tradeoff between accuracy and efficiency. The pioneering model is the ANN yawed wake model proposed by Ti et al. [19,20], which has been well-tested on the standalone and multiple wake predictions. A preliminary exploration by the authors further extends the ANN wake model to the yawed condition and verifies its efficacy in the power prediction and improvement of a simplified five-aligned turbine row in contrast with the analytical yawed wake model by Qian & Ishihara [21]. However, it has not been well applied to large-scale wind farms.

Besides the high-fidelity wake characterization, scholars have explored the rapid power optimization of large-scale wind farms. As a high-dimensional optimization problem, the real-time wind farm control puts higher demands for convergence rate than the layout optimization, indicating that the search-based optimization algorithms showing decent performance in the layout design, such as algorithm (GA) [22–24] and particle swarm optimization algorithm (PSO) [25,26], seem not to be a desirable tool for the yaw optimization. Although the above search-based optimization algorithms are applied to some research on wake steering strategies, most studies have focused only on power enhancement but hardly deal with the discussions on their computational efficiency [17,27,28]. Similarly, other algorithms employed before, like game theory and gradient descent algorithms, are confronted with the problem of low computational efficiency in real-time cooperative control [1,28–31]. Recently, some research has investigated the feasibility of using the Bayesian ML framework to realize real-time wind farm control, which is capable of finding the optimum state with limited data owing to the simultaneous accomplishment of learning and optimization at each iteration [32,33]. However, the previous study on improving the optimization efficiency is mainly confined to the optimization algorithm and lacking in discussions on the control scheme of wind farms concerning the decrease of the problem dimension. Some wind farm clustering approaches have ever been proposed, where each clustered subset is regarded as an independent control system [34–37]. Nevertheless, the complicated partition method using the wake digraph and the successive optimization of each subset add extra computational time to real-time cooperative control. Meanwhile, independent optimization of different subsets will ignore the wake interference between them and thus question the optimum of the final optimization result. Moreover, such partition methods cannot effectively harness the characteristics of the typical regular layout to improve overall optimization efficiency. Even though the iteration number in the Bayesian ML algorithm remains affordable for the yaw optimization of the current scale wind farm, it is still imperative that the developed double-layer ML framework can find the optimum control actions more rapidly in real-time large-scale wind farm control. Under such circumstances, some novel control schemes are in urgent demand, which can substantially decrease the optimization dimension through

the appropriate wind farm zoning based on the wake interaction pattern.

This study presents a novel double-layer ML framework comprising a yawed wake model using Artificial Neural Networks and an optimization algorithm based on Bayesian ML for cooperative wind farm control. RANS/ALM simulation with an improved  $k$ - $\epsilon$  turbulence model is utilized to generate enormous wake flow data to feed the ANN for accurate yawed wake prediction, thus the wind farm power prediction in an acceptable time, working as the 1st layer. The 2nd layer of the framework adopts the efficient Bayesian ML algorithm to conduct the yaw optimization calling the ANN-based power prediction data in the 1st layer. The developed framework is deployed to a 16-turbine wind farm. Considering the control on the iteration number with the scale-up of the wind farm, a novel row-based control scheme is developed to reasonably reduce the optimization parameters and then compared with the general independent control scheme. Two parametric studies are conducted with varying wind distributions and layout configurations to assess the performance of the row-based control scheme. Meanwhile, a further evaluation of the proposed control scheme is also conducted in a larger 49-turbine wind farm. Through comparing the effects of these factors on the discrepancies in power gain between the row-based and independent control schemes, recommendations on the applicability of the row-based control scheme to engineering practice are made, with different wind distributions and layout designs into consideration.

## 2. Double-layer ML control framework

### 2.1. ANN-based power prediction of wind farm

#### 2.1.1. Wake data preparation

High-fidelity RANS/ALM simulation is an ideal tool for generating an enormous wake flow dataset to feed the ANN yawed wake model, which has been fully validated in the reference [19] for wake modeling. To cover the full range of turbine operational conditions, a series of inflow conditions and yaw states are selected to guarantee the data sufficiency for ML model training, as listed in Table 1. Given the concrete site situation and the effect of turbine wake, the inflow hub-height velocity  $u_{\text{hub}}$  ranges from 5 m/s to 15 m/s, spacing 1 m/s, and the turbulence intensity  $I$  covers a range of 2% – 26% at 2% intervals. As the wake fields under the same positive and negative yaw angles exhibit symmetric, only the positive yaw-offset angle is accounted for in the dataset generation, varying from 0° to 30° at 3° intervals. Therefore, a sum of 1443 RANS/ALM coupling simulations are performed for enormous dataset production, among which 70 samples are picked up as the testing dataset, and the remaining are harnessed for model training.

Following the domain size of the RANS/ALM coupling simulation in the reference [21], the CFD model in Fig. 1 (a) and (b) is large enough to contain the majority region of the wake effect while alleviating the computational burdens at the same time. The axial and lateral ranges of the simulation domain are  $28D$  and  $12D$ , respectively. The snappy-HexMesh utility [38] employed in the present meshing can implement a smooth transition between two cells with marked size discrepancies through hexahedra and split-hexahedra mesh, which accomplishes the reduction of grid number while keeping the numerical stability.

#### 2.1.2. ANN yawed wake model for standalone turbine

As mentioned before, Artificial Neural Networks (ANN) establish an invisible black box bridging input and output layers through a back-propagation (BP) learning algorithm to make a compromise between

**Table 1**  
CFD simulation conditions for wake dataset generation.

	Range	Spacing	Number
Inflow velocity $u_{\text{hub}}$ (m/s)	5–15	1	11
Inflow turbulence intensity $I$	2% – 26%	2%	13
Yaw angle $\gamma$ (°)	0–30	3	11

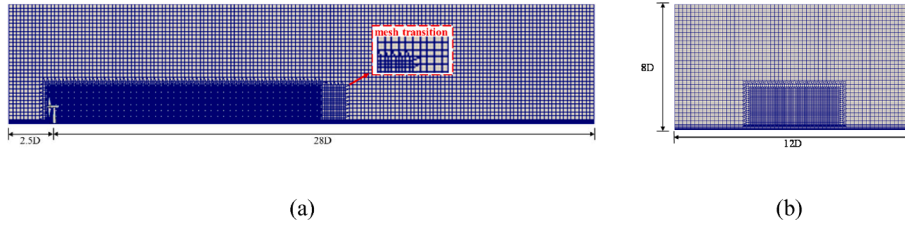


Fig. 1. CFD model mesh: (a) x-z plane; (b) y-z plane.

accuracy and efficiency [39]. As for the yawed wake prediction in this study, the ANN architecture is designed as shown in Fig. 2, where the input layer and output layer are bridged by the hidden layer connected with the weight matrix. The ANN training can be viewed as the dynamic tune of the weight matrix in the hidden layer to make the error between ANN prediction and target value satisfy the convergence requirements, namely, the evaluation of the loss function. The wake velocity and turbulence intensity predictions are achieved with the aid of two independent ANN models, where input variables are both  $u_{hub}$ ,  $I$ , and  $\gamma$ , while the output is the velocity deficit  $\Delta u$  and added turbulence intensity  $I_{add}$ , respectively. To accelerate the ANN training and fully harness the advantage of parallel computing, the wake field is further partitioned into  $N$  sub-fields along the transverse direction, which will be trained in independent ANN sub-models, respectively. Regarding each sub-model, the hidden layer contains ten neurons with the “sigmoid” activation function, and the loss function is optimized utilizing the Adam algorithm [40]. The final reproduction of the whole wake region is executed by integrating each sub-model prediction.

2.1.3. Multiple wake superposition

As for the cooperative yaw control of the large-scale wind farm, power maximization often serves as the optimization target. Therefore, besides the preliminary validation of the wake prediction for the standalone wind turbine mentioned above, more validation work on the wind farm power prediction is also in need, namely, the wake superposition prediction for multiple turbines. Generally, the downstream

turbine is under the wake influence regions of multiple upstream turbines, thereby calling for some superposition models combining the wake effect of all upwind standalone wind turbines. This study adopts the sum of square superposition model for  $\Delta u$  [41] but the linear superposition model for  $I_{add}$  in accordance with the energy conservation [42]. Thus, the wake velocity  $u_i$  and turbulence intensity  $I_i$  at turbine  $i$  can be computed as follow:

$$\left(1 - \frac{u_i}{u_{inflow}}\right)^2 = \sum_{j=1}^n \left(1 - \frac{u_{ij}}{u_j}\right)^2 \tag{1}$$

$$I_i^2 - I_{inflow}^2 = \sum_{j=1}^n I_{add,ij}^2 \tag{2}$$

where  $n$  denotes the quantity of the upwind turbines for turbine  $i$ ,  $u_{ij}$ , and  $I_{add,ij}$  are the wake velocity and added turbulence intensity at turbine  $i$  pertinent to the upwind turbine  $j$ , respectively. Combining the above superposition models with the proposed ANN yawed wake model, the overall wake field prediction can be achieved successively from the upstream to the downstream turbines, thus the total power prediction.

2.2. Bayesian ML for cooperative power control of wind farm

The focus of the real-time cooperative control of the large wind farm lies in the fast search for optimally coordinated control actions based on the measured wind data. As mentioned, the Bayesian ML framework exhibits better performance over traditional search-based optimization

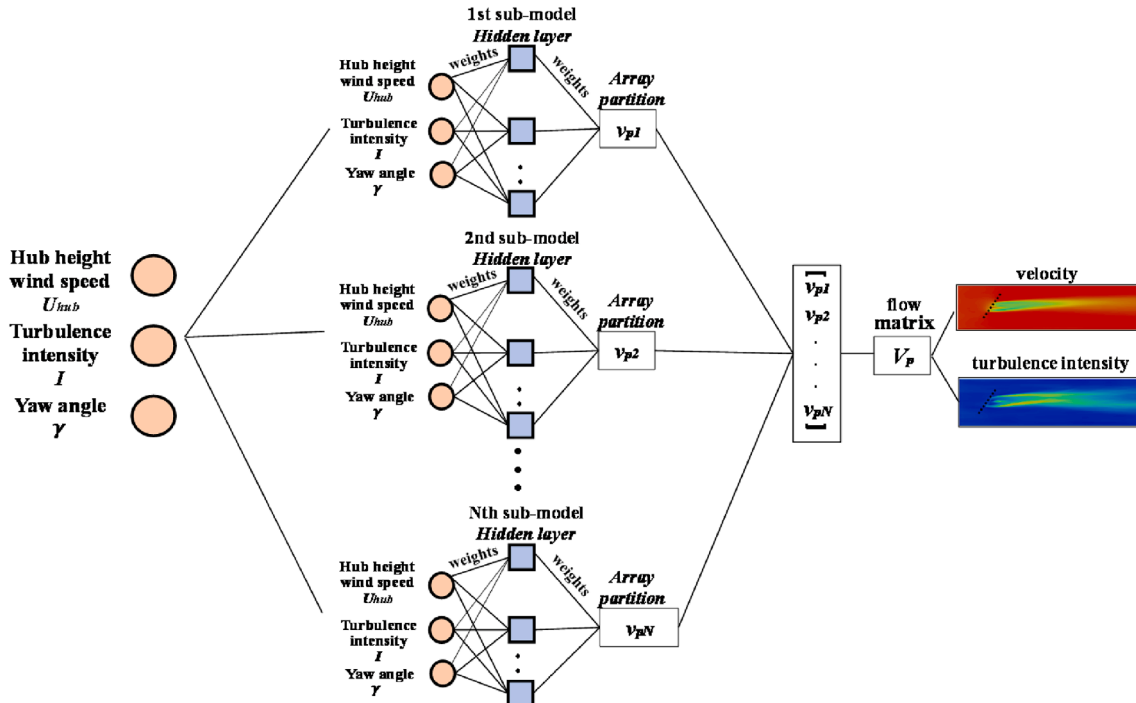


Fig. 2. ANN architecture for yawed wake prediction.

algorithms in terms of optimization efficiency, requiring a limited number of sampling points before reaching an optimal operational condition. In each optimization iteration, two targets, learning and optimization, are accomplished, that is to say, a more accurate characterization of the target function and continuous improvement of the target value. From the perspective of the superiority mentioned above, the Bayesian ML framework will be applied to the cooperative wind farm control in collaboration with the ANN-based power prediction framework. In more detail, this optimization problem can be defined as:

$$\begin{aligned} \text{maximize } f(\gamma) &= \sum_{i=1}^N P_i(u_{hub}, I, \gamma_i) \\ \text{subject to } &-\pi/6 < \gamma_i < \pi/6 \end{aligned} \quad (3)$$

where  $N$  denotes the quantity of the wind turbine,  $\gamma_i$  and  $P_i$  are the yaw angle and power output of the  $i$ th turbine, respectively. For each iteration in the Bayesian ML algorithm, the newly selected control input  $\gamma$  and the corresponding total power output  $P_{total}$  obtained from the ANN-based power prediction framework will compose a new dataset and then be contained in the existing training data  $D$ . In the learning phase, the probabilistically approximated relationship between  $\gamma$  and  $P_{total}$  is established using a Gaussian Process (GP) regression and the optimization of the hyperparameters  $\theta$  in the multivariate Gaussian distribution is conducted as follows:

$$\theta^* = \arg\max_{\theta} \log p(P_{total}^{1:n} | \gamma^{1:n}, \theta) \quad (4)$$

Based on the training data  $D$  and optimum hyperparameters  $\theta$  mentioned above, the posterior probabilistic distribution of the overall power prediction for a new yaw set  $\gamma$  satisfies a 1-D Gaussian distribution:

$$P_{total}(\gamma | D^n, \theta^*) \sim N(\mu, \sigma^2) \quad (5)$$

where  $\mu$  and  $\sigma^2$  symbolize the mean and variance, respectively. In the optimization phase, the next control input  $\gamma^{n+1}$  is searched based on two principles, the maximum expected value ( $\mu$ ) or uncertainty  $\sigma^2$ , which can be implemented by the following expected improvement (EI) acquisition function using the above derived posterior probabilistic distribution [43]:

$$\gamma^{n+1} = \arg\max_{\gamma} EI(\gamma) \triangleq E[\max\{0, P_{total} - P_{total}^{max}\} | D^n] \quad (6)$$

More details on the application of Bayesian ML to the current problem can refer to the literature [19].

A novel double-layer ML framework for cooperative wind farm control is established in this study, as shown in Fig. 3. In the 1st layer, the developed power prediction framework, combining the ANN yawed

wake model and some superposition models, can realize a prediction of the overall wake flow and power production with desirable accuracy and efficiency. In the 2nd layer, Bayesian machine learning can locate the optimally coordinated control actions of the wind farm rapidly using a few sampling points. For each optimization iteration process, the newly selected control input in the 2nd layer is delivered to the 1st layer to obtain the corresponding power output, both of which will compose a new dataset and then be contained in the training data  $D$  in the 2nd layer. The data feed from the 1st layer will help the 2nd layer to learn and optimize its target function at the same time. In summary, the developed double-layer ML framework can rapidly respond to real-time wind data owing to two favorable characteristics: power prediction and control optimization systems with a desirable tradeoff between accuracy and efficiency, and thus has great potential in the cooperative control of large-scale wind farms.

In this study, the complexity of the optimization problem increases with the number of wind turbines in the wind farm. Although the number of iterations in the Bayesian machine learning algorithm may remain affordable for the control optimization of the current wind farm in contrast with the exponential growth in the search-based optimization algorithm, it is still imperative that the developed double-layer ML framework is able to further improve the target value rapidly with the upscale of the wind farm. The previous studies revealed that the wake effect is localized in the downstream region along the axial direction, whereas the downstream turbines sited over a certain offset distance to the axial wake chain almost withstand insignificant power loss [44,45]. Given the above observations and the minimum constraints on the turbine separation distance in the current regular layout, a novel row-based control scheme will be developed to reasonably reduce the optimization parameters and then compared with the general independent control scheme in terms of optimization effect and efficiency.

As for the general wind farm, Fig. 5 demonstrates the layouts of row-based and independent cooperative control schemes, respectively. A set of parallel lines are drawn perpendicular to the wind direction and through all the turbine positions, defining the forefront as the baseline. The wind farm is equally decomposed into  $m$  rows along the wind direction, and each row consists of the turbines sited a specific range of offset distance to the baseline. For the row-based control scheme shown in Fig. 5(a), the turbines in each row are controlled by the same yaw angle based on the assumption that the wake interference within the same row is negligible and their effect on the downstream turbines is approximately the same. Note that the last turbine is under unyawed condition. To be specific, taking the turbine  $W_k$  in Fig. 4(a) as the

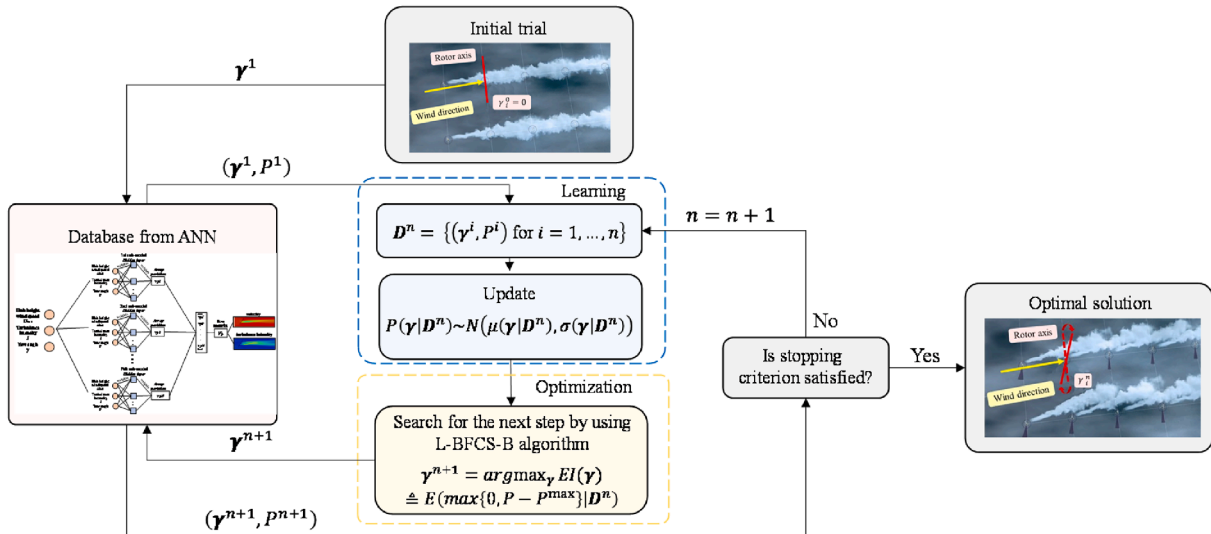


Fig. 3. Structure of Bayesian machine learning framework.

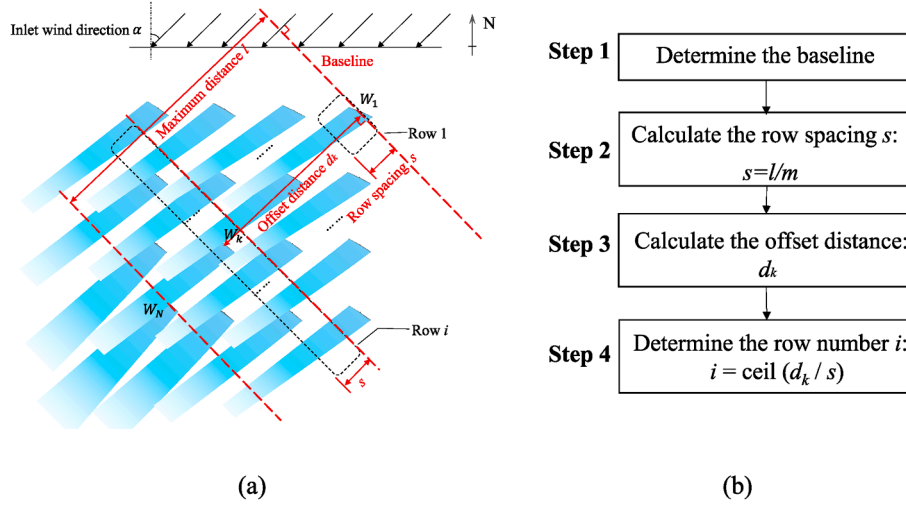


Fig. 4. Determination of row number: (a) example turbine  $W_k$  in the wind farm; (b) flowchart of the determination process.

example, the row number  $i$  of turbine  $W_k$  in the wind farm can be determined by the following steps:

Step 1: Draw a set of parallel lines perpendicular to the wind direction and through all the turbine positions, and define the forefront as the baseline, corresponding to the first turbine  $W_1$ .

Step 2: Define the maximum distance between other parallel lines and the baseline as  $l$ , corresponding to the last turbine  $W_N$ , and calculate the row spacing  $s$  based on  $l$  and the prescribed total row number  $m$ .

$$s = \frac{l}{m} \quad (7)$$

Step 3: Calculate the offset distance of the turbine  $W_k$  to the baseline  $d_k$ .

Step 4: Determine the row number  $i$  of the turbine  $W_k$ .

$$i = \text{ceil}(d_k/s) (i = 1, 2, \dots, m) \quad (8)$$

where function  $\text{ceil}()$  returns the smallest integer not less than the value in the bracket(). The determination process is illustrated in a flowchart, as shown in Fig. 4(b).

For the general independent cooperative control scheme shown in Fig. 5 (b), the yaw misalignment of each turbine is an independent optimization variable with no extra constraints imposed except for the last turbine along the wind direction remaining unyawed. Therefore, it is clear that the row-based control scheme reduces the dimension of the optimization parameter  $\gamma$  from the total turbine number  $N$  to the row number  $m$ , relieving an excessive number of iterations and possessing a paramount potential in the real-time cooperative yaw control of a large number of wind turbines.

Therefore, the comprehensive control process can be illustrated using the flowchart in Fig. 6, consisting of two stages. In Stage 1, according to the wind farm layout and inflow conditions, an appropriate wind farm partition is deployed to the selected wind farm, dividing it into several rows. Stage 2 determines the optimal cooperative control action using the double-layer machine learning framework combining with the row-based control scheme. Note that the wind farm partition method introduced above is implemented based on the regular layout discussed in this study. As for the irregular layout, precisely the optimal layout, the optimized wind farm partition method will replace the simple one mentioned above to assist the row-based control scheme in realizing a power enhancement equivalent to the independent one. This

control framework comprising two successive optimization systems will be explored in depth in the future study.

### 3. Validation of the ANN model

#### 3.1. Standalone wind turbine

To evaluate the accuracy of the trained ANN model, the testing dataset containing 70 samples mentioned above is adopted to compare the ANN model predictions and actual CFD data, as shown in Fig. 7, supplemented with the correlation coefficient as a quantitative index. The decent data match and high correlation coefficient indicate that the trained ANN yawed wake model can realize a high-quality prediction of a standalone wind turbine wake field commensurate with CFD data.

To gain a more intuitive insight into the precision of wake modeling using the proposed ANN yawed wake model, contours of velocity and turbulence intensity at the hub height are extracted. The inflow and operational conditions are selected as  $u_{hub} = 8 \text{ m/s}$ ,  $I = 7.7\%$ ,  $\gamma = 30^\circ$ . The relative error between the ANN model and CFD simulation is defined as:

$$\text{Relative error} = \frac{Y_{ANN} - Y_{CFD}}{Y_{CFD}} \times 100\% \quad (9)$$

where  $Y$  represents the spatial velocity or turbulence intensity. Fig. 8 illustrates the results of the ANN yawed wake model, CFD simulation, and relative error, it is observed that the ANN model can predict the yawed wake structure for a standalone wind turbine with appreciable accuracy. The majority of errors concentrate in the near wake area, especially near the blade tip, owing to the strong disturbance of the inflow by the rotor in this area. In general, the errors are below 5%, regardless of the wake velocity and turbulence intensity, proving the decent capability of the proposed ANN model in predicting the yawed wake field.

#### 3.2. Multiple aligned turbines

The ANN yawed wake model has been well validated for the standalone wind turbine in the above section, then its efficacy of wake predictions on multiple turbines needs to be further justified. The two aligned turbines are selected, where the first turbine is operated at the yaw angle of  $30^\circ$  and the second one is under the unyawed condition. Fig. 9 illustrates the hub-height velocity and turbulence intensity fields and the comparison between the ANN predictions and RANS/ALM coupling simulation. It can be seen that the ANN yawed wake model collaborating with some superposition models, can correctly predict the

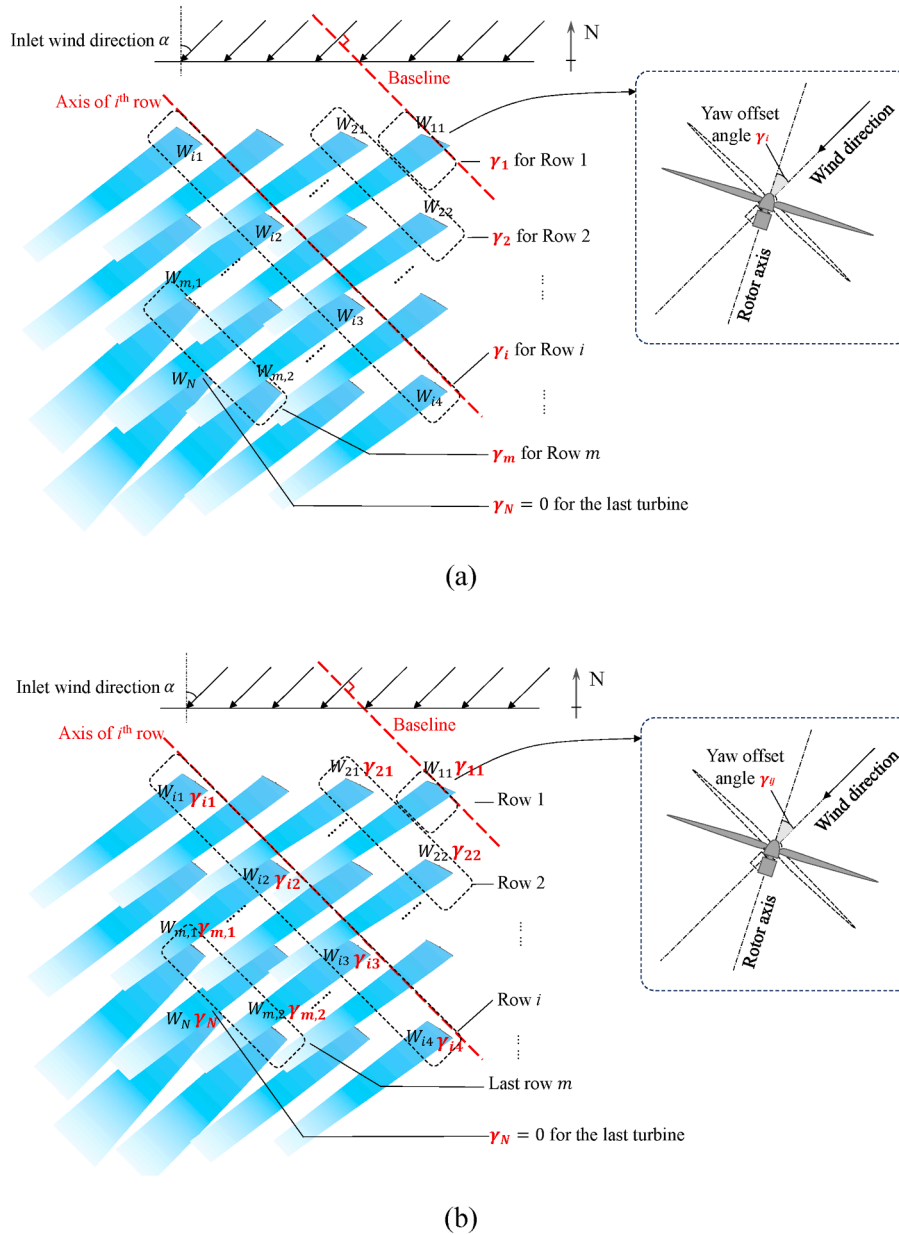


Fig. 5. Cooperative yaw control of wind farm: (a) row-based cooperative control scheme; (b) independent cooperative control scheme.

wake structure of multiple turbines involving the velocity and turbulence intensity fields. Due to the intuitive defects of the empirical wake superposition models, there is inevitably a tiny increase in error compared with the above wake prediction for the standalone turbine. Even though the proposed framework imposes errors up to 20% in the velocity fields and about 10% in the turbulence intensity field, the significant errors mainly concentrate immediately in front of and behind the turbine or at the blade tip, and the inflow velocity of each turbine at the hub height can still be captured accurately, leading to a relatively precise power prediction. The significant errors right in front of the 2nd turbine result from the ignorance of disturbance of the turbine rotating to the surrounding flow field, specifically the region just in front of the turbine, when employing the wake superposition based on the wake model for the standalone turbine. The wake models, including the ANN or analytical models, only consider the flow field behind the turbine, while the CFD simulation can show the effect of the turbine rotating on the surrounding flow field, including the front area. Therefore, the general errors are within 10% in most wake regions, revealing that the

proposed ANN-based framework works well in the wake predictions of the multiple turbines, namely, the modeling of turbine interaction.

### 3.3. Wind farm power production

To shed light on a comprehensive evaluation of the ANN-based power prediction framework, the high-fidelity LES data concerning the total power output of the Horns Rev wind farm in the literature [46] are used for comparison, covering a wide range of wind directions varying from  $180^\circ$  to  $360^\circ$ . Various wind directions are accounted for, including the full-wake and partial-wake conditions, and the counterpart based on the analytical yawed wake model by Qian & Ishihara is also supplemented as another comparison index, as shown in Fig. 10. From Fig. 10, it is evident that both models perform favorably in the overall power prediction of the wind farm under various wake conditions, where the ANN-based power prediction is more advantageous than the analytical one. Although there ubiquitously exists a slight overestimation of the power in contrast with the LES data, satisfactory accuracy can be

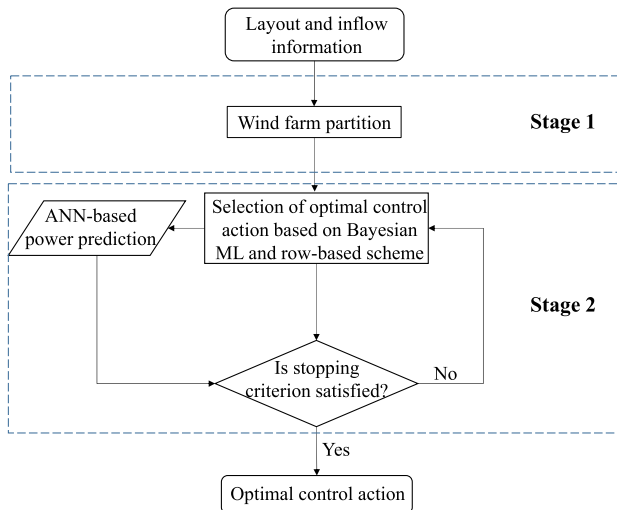


Fig. 6. Comprehensive two-stage control flowchart.

guaranteed, especially for the wind direction near the full-wake condition. The insignificant deviation of the two wake models from the LES data under the partial-wake conditions can be explained by the ignorance of the wake fringe region in both wake models. To sum up, the above validation works fully justify the reasonability and feasibility of the proposed ANN-based power prediction framework in real-time cooperative wind farm control application.

#### 4. Case studies

The total power output prediction of the wind farm based on the 1st layer in the proposed double-layer ML framework has been validated, then the performance of the Bayesian ML in the 2nd layer is investigated by applying it to the real-time cooperative wind farm control. The preliminary results concerning the optimal cooperative control of a simplified five-aligned turbine row can refer to the literature [21], where the proposed framework has a significant advantage in the power prediction and enhancement for this small-dimension optimization problem compared with the analytical yawed wake model by Qian & Ishihara. The more complex application will be implemented in the scale wind farm simplified from the Horns Rev wind farm. This scaling keeps the original layout feature without losing generality and effectively reduces the optimization cost. Based on the complete validation of the total power prediction for the Horns Rev wind farm under varying wind directions in section 3.3, the 16-turbine wind farm with four by four aligned layout simplified from its original turbine layout is deployed to compare the two cooperative control schemes mentioned above, as

shown in Fig. 11.

According to the meteorological measurements taken at the realistic weather station, the wind speed and direction data display a joint probability distribution. Such wind characteristics play an indispensable role in evaluating the wind resource and the design and operation of the wind farm. Therefore, besides the basic single wind direction, two typical wind direction distributions, the uniform wind direction and general wind rose, as shown in Fig. 12, are also included in the following discussion to investigate the effect of the probability density distribution of the wind speed on the effectiveness of the row-based cooperative control scheme.

Another critical issue worth discussing lies in the effect of turbine layout configuration on the power improvement of different control schemes, where the layout design is often conducted in the initial stage to improve the efficiency of the wind farm without the consideration of the yaw control in the operation stage. The commonly-adopted regular arrangements in the current wind farm usually include two patterns, aligned and staggered layouts, among which the staggered layout shows a better performance in the wake mitigation and power capture than the aligned one considering the unyawed control of the wind farm. Hence, a new staggered layout, as shown in Fig. 13, is also created by sliding the 2nd and 4th rows in the aligned arrangement mentioned above with half of the turbine spacing to compare the distinction of the power growth that the yaw control strategy brings, as the counterpart of the aligned layout.

## 5. Results and discussions

### 5.1. Comparison of two cooperative control schemes in the aligned layout

#### 5.1.1. Single wind direction

Considering the aligned wind farm layout with four by four, as shown in Fig. 11, the row-based control scheme partitions the wind farm into four rows along the wind direction, and turbines within the same row interact weakly through wakes. The double-layer ML framework is then applied to the target wind farm based on the row-based and independent cooperative control schemes, respectively. Under such circumstances, the dimension of the optimization parameter will see a remarkable fall from fifteen in the independent cooperative control scheme to four in the row-based cooperative control scheme. Fig. 14 (a) and (b) display the optimized yaw angles based on the two cooperative control schemes under wind direction  $270^\circ$ . The optimized yaw-angle distribution in the row-based control scheme exhibits a decreasing trend with the row number, especially from the 2nd row to the 3rd row, indicating that the sacrifice of the power capture of the first two rows mitigates the power loss of the last two rows incurred from the wake interference. A similar decreasing trend of yaw angle from the upstream turbines to the downstream one can also be observed in the independent cooperative control scheme, but the middle two turbines in the 2nd row

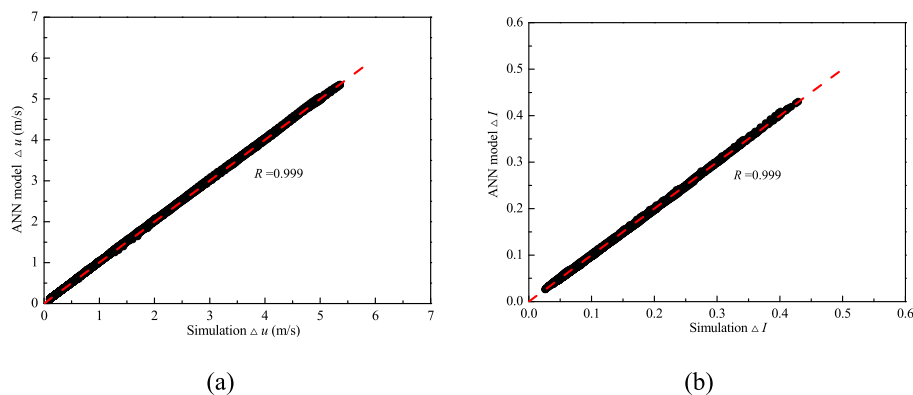
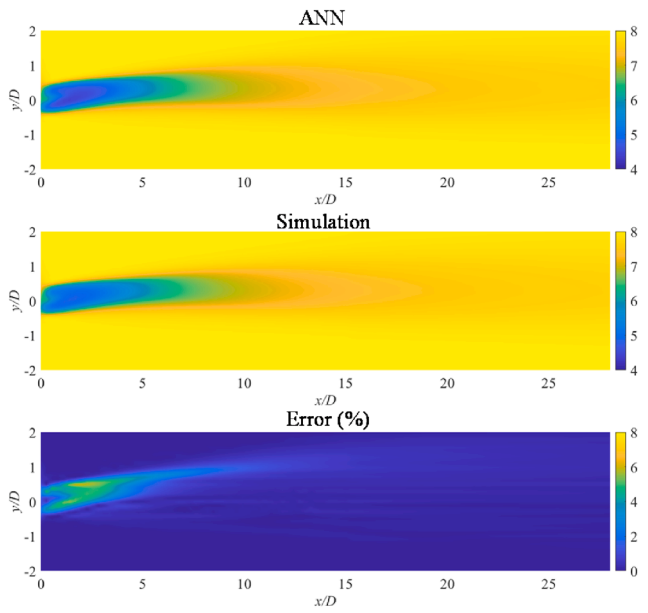
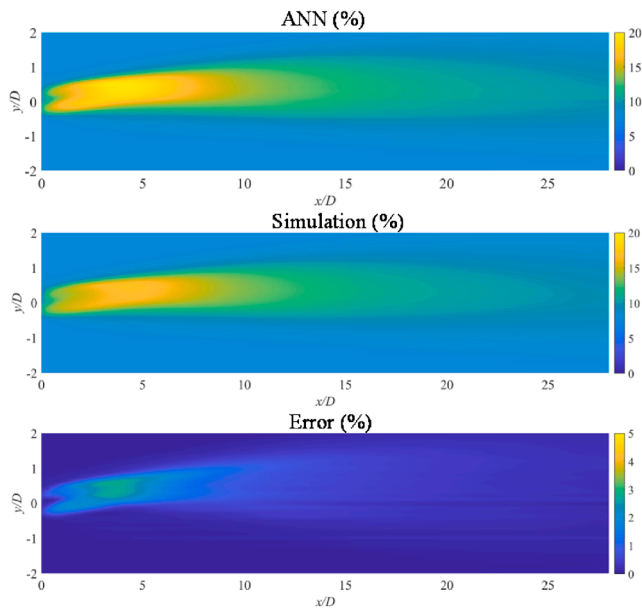


Fig. 7. Wake prediction comparison between the ANN model and the CFD simulation: (a) velocity deficit; (b) added turbulence intensity.



(a)

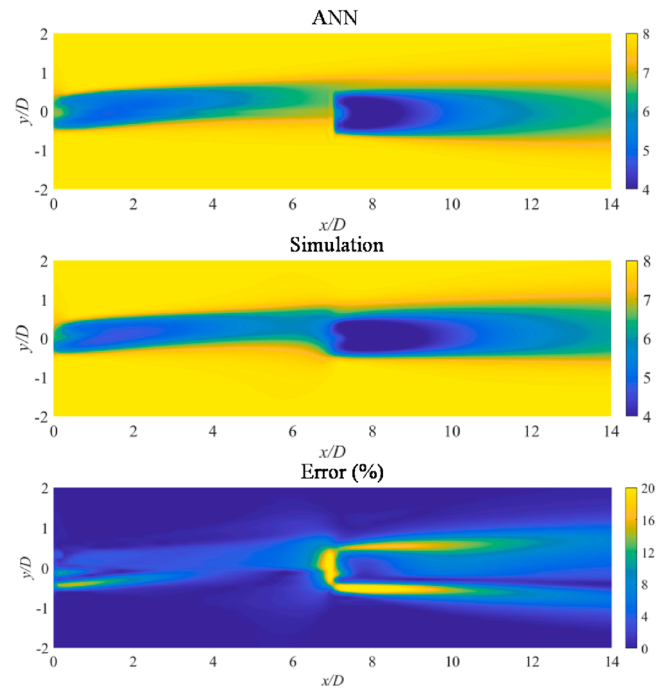


(b)

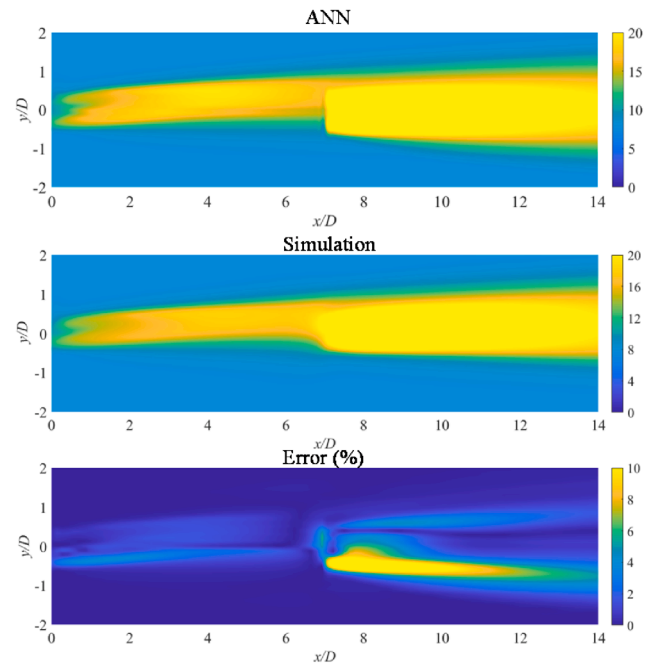
**Fig. 8.** Comparison of ANN model predictions and RANS/ALM coupling simulation results for standalone wind turbine: (a) spatial velocity; (b) spatial turbulence intensity.

are yawed with a smaller angle owing to the different yaw directions of the upstream turbines in the 1st row. Accordingly, there is a tiny increase in the yaw angle for the downstream turbines in the 3rd row. The above slight disparities of optimized yaw angle distribution between the two control schemes can attribute to the subtle wake interactions of the turbines within the same row and possible minor differences in their effects on the downstream turbines.

To obtain a direct view of the effect of the above optimal yaw control strategies, Figs. 15 and 16 illustrate the comparisons of the hub-height wake velocity and turbulence intensity based on the two cooperative



(a)



(b)

**Fig. 9.** Comparison of ANN model predictions and RANS/ALM coupling simulation results for two aligned turbines: (a) spatial velocity; (b) spatial turbulence intensity.

control schemes, where the related contour under the greedy control is also offered as a reference. It is shown that the two cooperative control strategies weaken the strong wake interaction under the greedy control significantly by deflecting the wake trajectory of the upwind turbines, manifesting a rise in wake velocity and a fall in turbulence intensity in front of the downstream turbines. Moreover, the independent cooperative control scheme induces a more noticeable impact on the downstream turbine rows than the row-based one, seeing an apparent

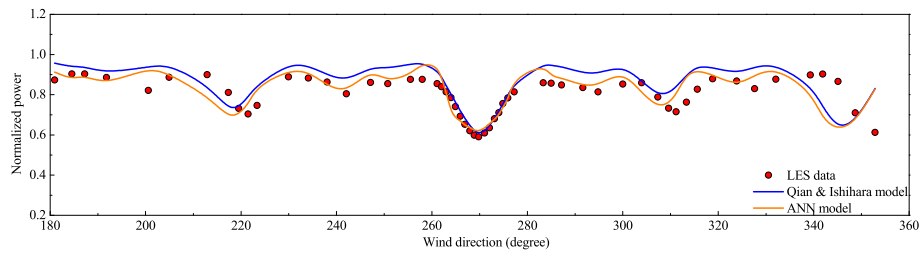


Fig. 10. Total power predictions using the ANN yawed wake model, Qian & Ishihara model, and LES.

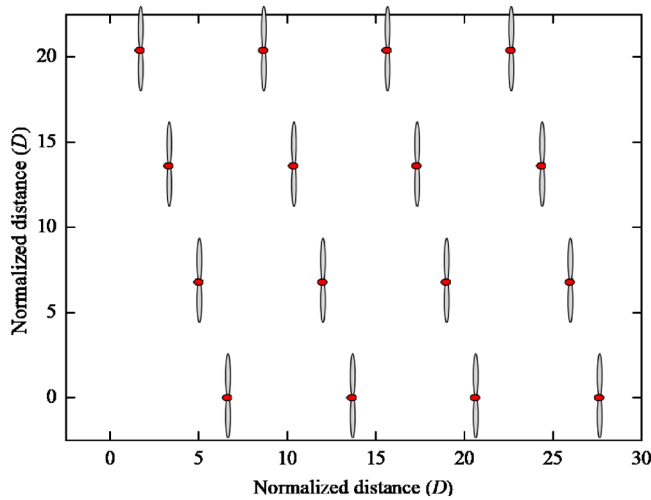


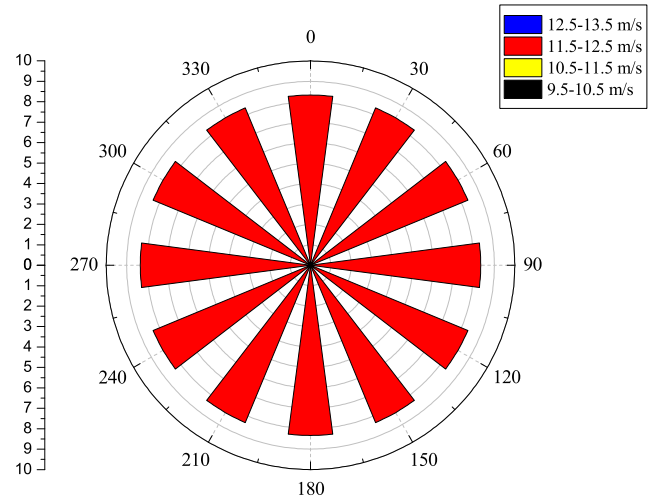
Fig. 11. Aligned wind farm layout.

discrepancy in wake flow fields in front of the turbines at the edge of each row.

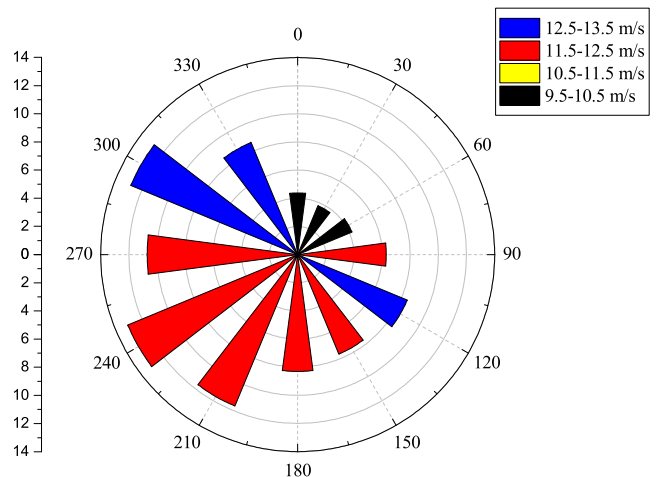
To compare the optimization efficiency and effect between the two cooperative control schemes quantitatively, Fig. 17 shows the variation of the overall power output with the iteration of the Bayesian ML, as well as the corresponding optimal target values. As shown in the figure, there is a stable increase of the target value with the iteration in the independent cooperative control scheme, reaching up to higher optimal power output of 22.32 MW at around 300 iterations than in the row-based control scheme. Nonetheless, the target value in the row-based cooperative control scheme only falls behind at the initial phase and then experiences a sudden upsurge to the optimal value of 22.26 MW at approximately 50 iterations. Even though the optimal power output in the independent cooperative control scheme leads to the one in the row-based cooperative control scheme slightly, its convergence rate lags far behind the row-based one, nearly 1/6. Moreover, for each iteration's local optimization problem (Eq. (6)), there also exist pronounced discrepancies in the consuming time for the row-based and independent cooperative control schemes owing to the variation of the parameter dimension. This difference further enhances the superiority of row-based control in optimization efficiency. Therefore, sacrificing the slight power output for a remarkable optimization efficiency in the row-based cooperative control scheme can be deemed a desirable tradeoff between efficiency and effect, thereby having the potential for broad application to the real-time cooperative control of the large-scale wind farm.

5.1.2. Uniform wind direction

Considering the uniform distribution of wind direction with the same wind velocity of 12 m/s as shown in Fig. 12(a), the wind direction is divided into 12 sectors with an angle range of 30°. The power rose in Fig. 18 illustrates the power output in each wind section under greedy control, row-based cooperative control, and independent cooperative control, respectively, which are all normalized by the power of the



(a)



(b)

Fig. 12. Wind direction distribution: (a) uniform wind direction; (b) wind rose.

standalone wind turbine under the undisturbed inflow. As far as the greedy control is concerned, apart from the wind sector 270° and its negative direction 90°, significant power drops also occur at the wind sector 240° and its negative direction 60°. At the same time, power output at the remaining wind sectors barely suffers from the wake loss. The above phenomena can result from the possible existence of the turbines under the full-wake or partial-wake regions of the upstream turbines at the wind sectors 270°, 90°, 240°, and 60°. Moreover, owing to the regularly aligned layout and the uniform wind direction distribution with the same wind speed, the power roses all exhibit a

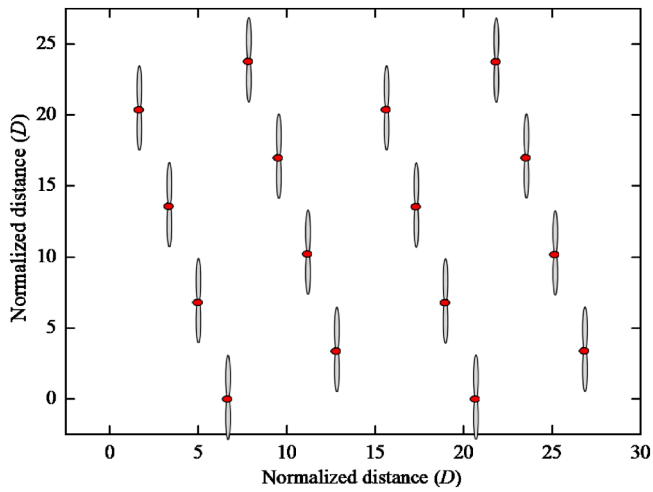


Fig. 13. Staggered wind farm layout.

symmetric distribution. When it comes to cooperative control, two optimization schemes both alleviate the power loss effectively at the wind sectors with the marked wake interference, among which more remarkable power enhancement can be observed at the wind sectors  $270^\circ$  and  $90^\circ$  than at  $240^\circ$  and  $60^\circ$ . This is because, at the former wind sectors, the regularly aligned layout creates more full-wake conditions, and thus the cooperative control is capable of mitigating the power loss

of more downstream turbines under these conditions. Nonetheless, at the latter wind sectors, the decrease of the turbine number under the full-wake conditions and the increase of the turbine spacing in the wake interaction region both limit the effectiveness of the wake steering strategy. On the other hand, the disparity of the power contributions between the row-based and independent optimization experiences a slight rise from the wind sectors  $270^\circ$  and  $90^\circ$  to  $240^\circ$  and  $60^\circ$ , possibly attributing to the enhancement of wake interaction between the turbines in the same row.

To gain a more insightful view of the discrepancies between the wind sector  $270^\circ$  and  $240^\circ$ , Fig. 19(a) and (b) further show the optimized yaw angles based on the two cooperative control schemes under wind direction  $240^\circ$ . As for the row-based control scheme, the optimized yaw misalignment sees a decreasing tendency similar to the one under wind direction  $270^\circ$  from the upstream turbines to the downstream one, while the yaw angles in the first two rows become smaller due to the weakening of the wake effect. Besides the above difference in the row-based control scheme, it is worth noting that the nearly no-wake deflection is in demand for the first column and the yaw angles of the other turbines in the first two rows almost remain the same for the independent control scheme. Furthermore, the rest turbines are all operated under unyawed conditions.

Hub-height wake velocity and turbulence intensity contours in Figs. 20 and 21 will aid in a better understanding of the mechanism behind the above control discrepancy. As shown in Fig. 20(a), the full-wake regions only cover the locations of the six downstream turbines, which explains why there appears to be a minor power loss at this wind sector than at the wind sector  $270^\circ$ . In addition, the increase in the

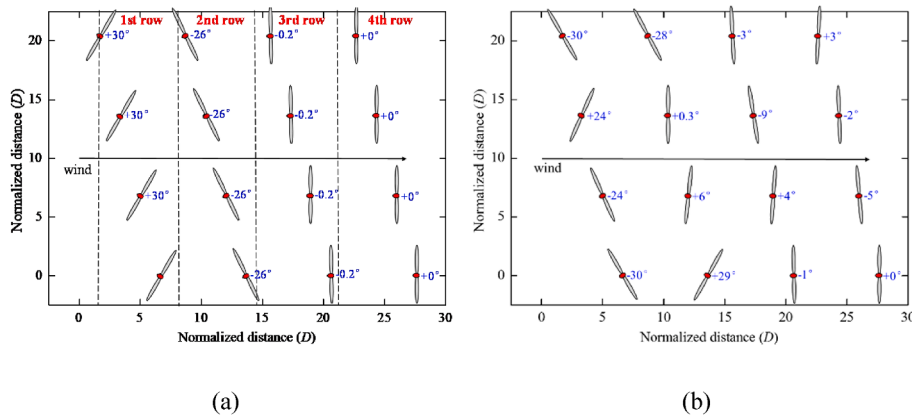


Fig. 14. Optimized yaw angles for aligned layout under wind direction  $270^\circ$ : (a) row-based control scheme; (b) independent control scheme.

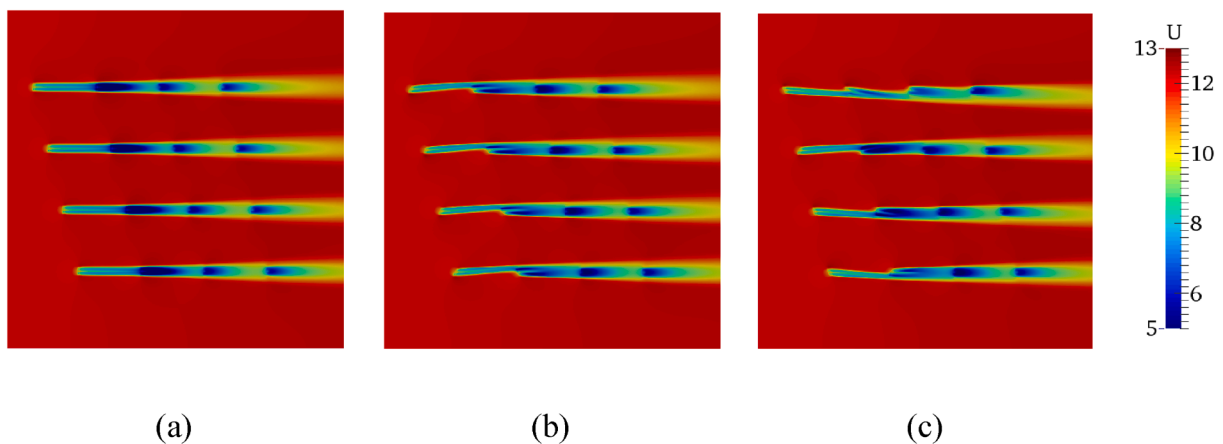


Fig. 15. Contours of velocity for aligned layout under wind direction  $270^\circ$ : (a) greedy control; (b) row-based control optimization; (c) independent control optimization.

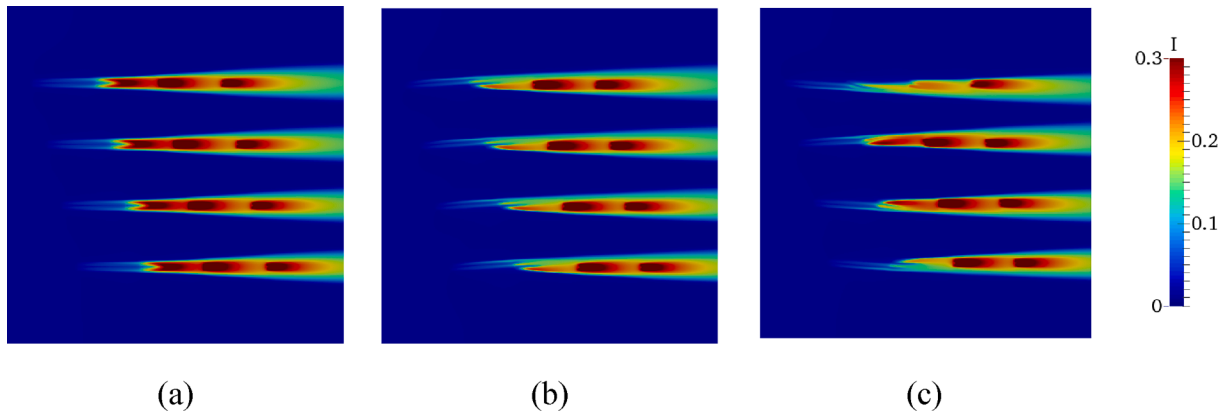


Fig. 16. Contours of turbulence intensity for aligned layout under wind direction 270°: (a) greedy control; (b) row-based control optimization; (c) independent control optimization.

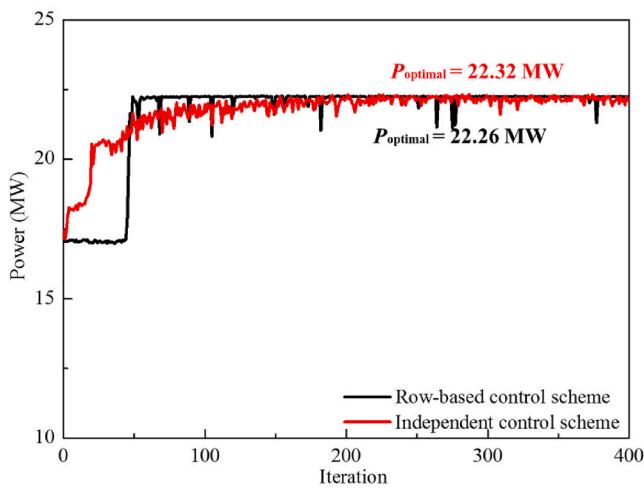


Fig. 17. Convergence comparison of two control schemes.

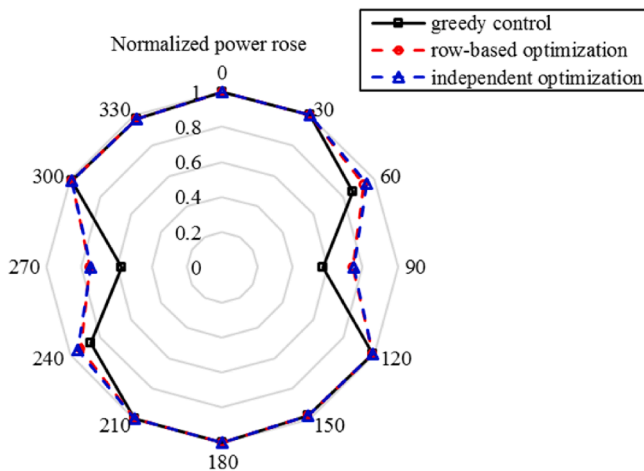


Fig. 18. Power rose diagram for aligned layout under uniform wind direction.

turbine spacing pertinent to the full-wake effect can bring on a sufficient distance for the wake recovery and, thereby, a less remarkable power gain resulting from the wake steering strategy. As for the difference in the control scheme in Fig. 20(b) and (c), the extra constraints on the yaw angle within the same row in the row-based control scheme will impair the effectiveness of the wake steering strategy. Even though the

power loss of the turbines under full-wake conditions can be made up for due to the deflection of the wake trajectories of the upwind turbines, the passive yaw of the other turbines, of which the wake effect on the downwind turbines is negligible, will lead to the meaningless sacrifice of their power output, thus the overall power drop of the wind farm. As seen in Fig. 20(c), the upstream turbines that impose no wake effect on the downstream turbines do not need to yaw to skew the wake under the independent control scheme, in contrast with the unified yaw of the first two turbine rows under the row-based control scheme in Fig. 20(b). Similar phenomena can also be observed in the hub-height turbulence intensity contours, as shown in Fig. 21.

### 5.1.3. Wind rose

The measured wind rose shown in Fig. 12(b), symbolizing a typical wind speed probability density distribution in the engineering practice, is employed to assess the performance of the different control schemes on the power and AEP (annual energy production) improvements. It is clear that the majority of winds come from the NW (North-West) and SW (South-West) directions, ranging from 11.5 m/s to 13.5 m/s. Fig. 22 further illustrates the power under greedy control, row-based cooperative control, and independent cooperative control in a rose diagram. Interestingly, the symmetric distribution of the power rose can still be observed under greedy control, whereas the cooperative controls induce apparent disparities in the power improvements at the symmetric wind sectors. Specifically, at wind sectors 270° and 90°, a smaller power rise occurs for the latter wind direction due to the slight decrease of the wind speed compared with the former wind direction. Similarly, the cooperative control strategies have nearly no power benefits at the wind sector 60° in contrast with substantial power gain at the wind sector 240°. This phenomenon is mainly because the operational speed limits the yaw of the turbines under low wind speed, which in turn influences the degree of the wake mitigation induced by the wake steering strategy and, thus, the overall power increase of the wind farm. On the other hand, the independent cooperative control scheme seems to bring a more positive effect to the power gain caused by the cooperative control than the row-based one at wind sector 90°, while there is a minor difference in power output between the row-based and independent cooperative control schemes at wind sector 270°. This can result from more significant wake interactions between the turbines within the same row and more enormous differences in their impacts on the downstream turbines.

### 5.1.4. Effect of wind direction distribution in the aligned layout

To make a quantitative comparison of the influence of the wind direction distribution on the effectiveness of the row-based cooperative control scheme, annual energy production (AEP) is employed to take the occurrence frequency of each wind sector into account and represent the energy production in a year for the uniform wind direction and wind

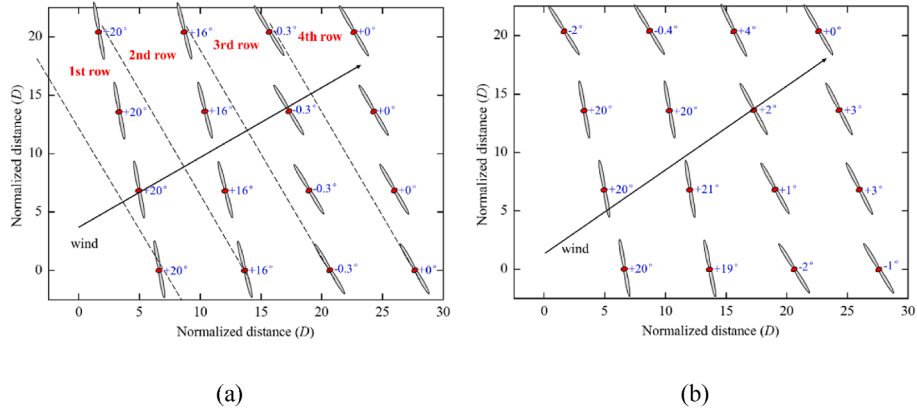


Fig. 19. Optimized yaw angles for aligned layout under wind direction 240°: (a) row-based control scheme; (b) independent control scheme.

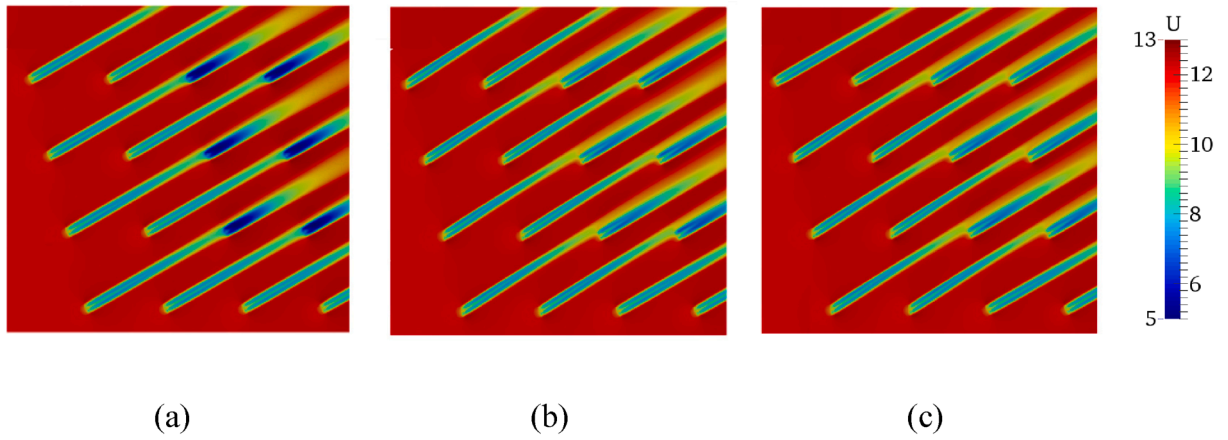


Fig. 20. Contours of velocity for aligned layout under wind direction 240°: (a) greedy control; (b) row-based control optimization; (c) independent control optimization.

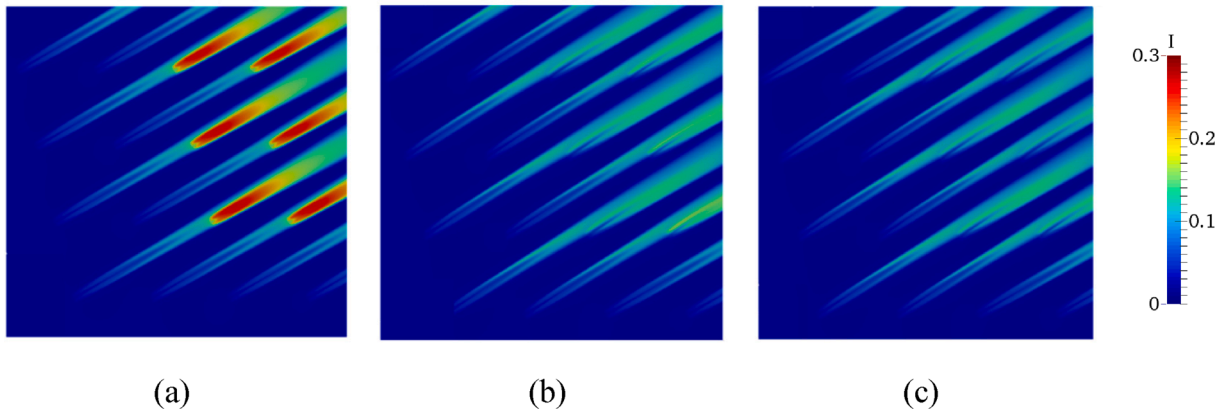


Fig. 21. Contours of turbulence intensity for aligned layout under wind direction 240°: (a) greedy control; (b) row-based control optimization; (c) independent control optimization.

rose, which can be calculated as

$$AEP = T \sum_{i=1}^N P_i \bullet f_i \tag{10}$$

where  $P_i$  is the power at wind sector  $i$ ,  $f_i$  is the corresponding occurrence frequency,  $N$  is the number of the wind sector, taking 12 in this study,  $T$  is the total time length. Table 2 lists the power increase ratio based on the two control schemes considering three wind direction

distributions, as well as their differences. With regard to the power gain of the cooperative control, the single wind direction brings a more considerable benefit, while there appears to be a substantial fall under the uniform wind direction and wind rose, where the uniform wind direction stands a little ahead of the wind rose. Conversely, the discrepancies in power enhancement between the row-based and independent cooperative control schemes experience a distinct upsurge under the uniform wind direction and wind rose compared with the single wind direction. Therefore, the divergence of the wind speed and direction can

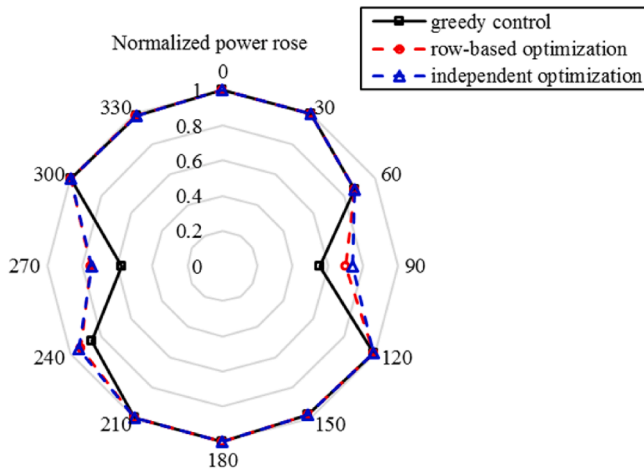


Fig. 22. Power rose diagram for aligned layout under wind rose.

Table 2

Comparison of two control schemes for aligned layout under three wind direction distributions.

Control scheme	Single	Uniform distribution	Wind rose
Row-based	30.0%	4.6%	4.3%
Independent	30.4%	4.9%	4.7%
Difference	1.33%	6.52%	9.22%

dwindle the benefits of the wake steering strategy and also weaken the superiority of the row-based cooperative scheme over the independent one.

### 5.2. Comparison of two cooperative control schemes in the staggered layout

#### 5.2.1. Single wind direction

As for the single wind direction, the optimized yaw angles in the staggered layout based on the row-based and independent cooperative control schemes are demonstrated in Fig. 23(a) and (b), respectively. A decreasing tendency of yaw angle from the upstream to the downstream can be observed for both cooperative control schemes, similar to the variation pattern in the aligned layout. However, in the staggered layout, the yaw offset angles of the first two rows see an evident fall compared with the ones in the aligned arrangement, and also, the last two rows nearly call for no wake skew. In addition, when it comes to the dissimilarity induced by the cooperative scheme, the turbines in the first two rows under the independent cooperative control scheme yaw almost

to the same degree, whereas a relatively distinct change of the yaw angle from the 1st to the 2nd row still displays under the row-based cooperative control scheme. Meanwhile, the yaw direction of the turbines in the 2nd row under the independent cooperative control scheme exhibits a positive-negative staggering trend.

A more comprehensive analysis of the effects of the above optimal wake steering strategies will be unfolded based on the hub-height wake velocity and turbulence intensity in Figs. 24 and 25. Note that the staggered arrangement of the adjacent rows creates additional passages for the passing through of the upstream wake and thus elongates the distance of the wake recovery. Meanwhile, the number of turbines under full-wake conditions experiences a substantial drop; specifically, the turbines in the 2nd row face the undisturbed inflow rather than the significant wake velocity deficit in the aligned layout. Consequently, when it comes to the case under greedy control, the staggered layout is somewhat capable of relieving the severe power loss owing to the complex wake interactions in the aligned layout. As far as the wake mitigation through the cooperative control strategy is concerned, the wake velocity deficit in front of the turbine bears a marked decline under the independent cooperative control scheme in contrast with the row-based one, accompanied by a fall in the turbulence intensity at the same time, especially for the last several turbine rows. The more apparent deviation between the two cooperative control schemes in the staggered layout can be explained by the disparities of the wake interference patterns on the downstream turbines between the turbines in the same row, typically for the middle and edge positions. Moreover, the narrowing down of the inter-column spacing incurred from the staggering of the consecutive row complicated the wake interaction between the turbines between different rows, which further undermines the rationality of the constraint on the unified yaw angle within the same row in the row-based cooperative control scheme.

#### 5.2.2. Uniform wind direction

The uniform wind direction in Fig. 12(a) is also employed to evaluate the efficacy of the two cooperative control schemes on the power enhancement in each wind sector for the staggered layout. Fig. 26 demonstrates the power rose under greedy control, row-based cooperative control, and independent cooperative control, respectively. When the wind farm is under greedy control, the primary power loss occurs at the wind sectors 240° and 60°, followed by the secondary one at the wind sectors 270° and 90°, whereas the aligned layout displays an opposite trend. Accordingly, the cooperative control strategy can contribute more to the power gain under the wind directions 240° and 60° than 270° and 90°, but bring ignorable power improvement to the rest wind directions, under which the wind farm suffers from a slight power loss. On the other hand, when it involves the efficacy difference between the two cooperative control schemes, the superiority of the independent cooperative control scheme over the row-based one

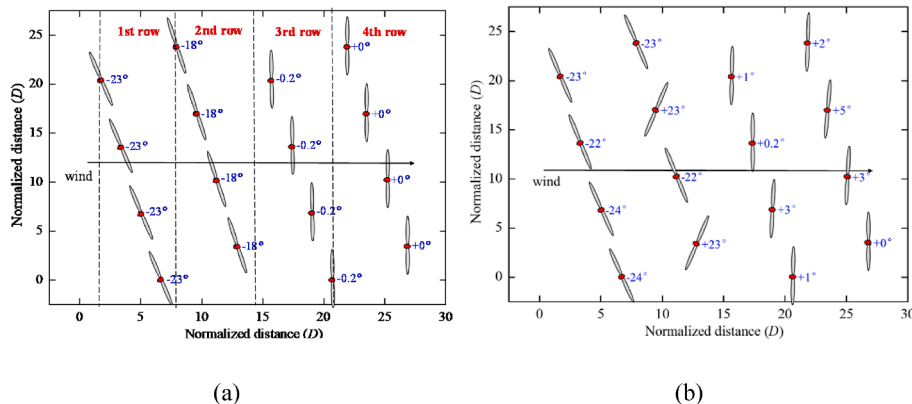


Fig. 23. Optimized yaw angles for staggered layout under wind direction 270°: (a) row-based control scheme; (b) independent control scheme.

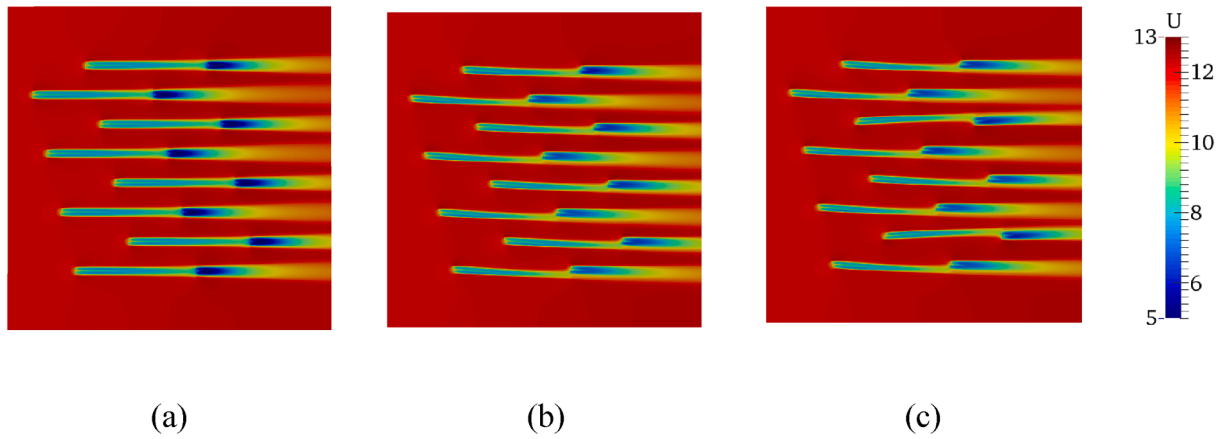


Fig. 24. Contours of velocity for staggered layout under wind direction 270°: (a) greedy control; (b) row-based control optimization; (c) independent control optimization.

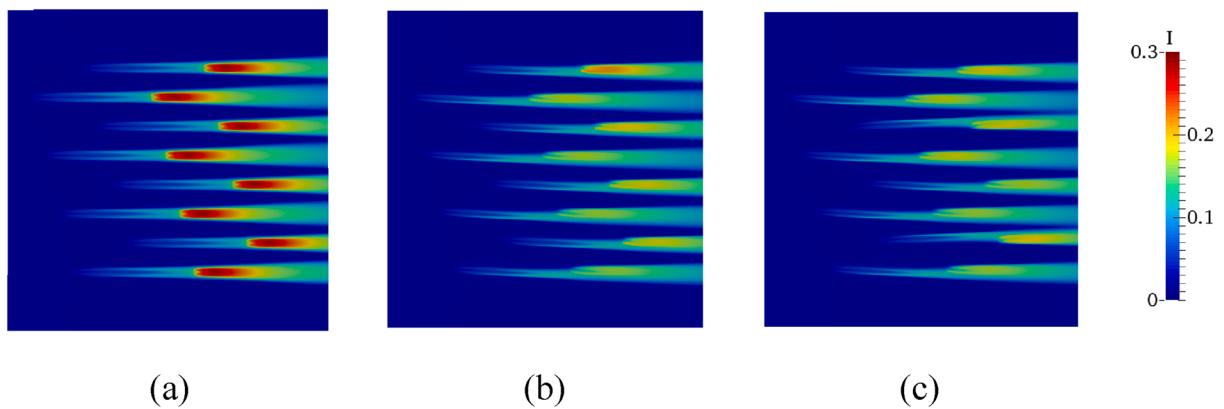


Fig. 25. Contours of turbulence intensity for staggered layout under wind direction 270°: (a) greedy control; (b) row-based control optimization; (c) independent control optimization.

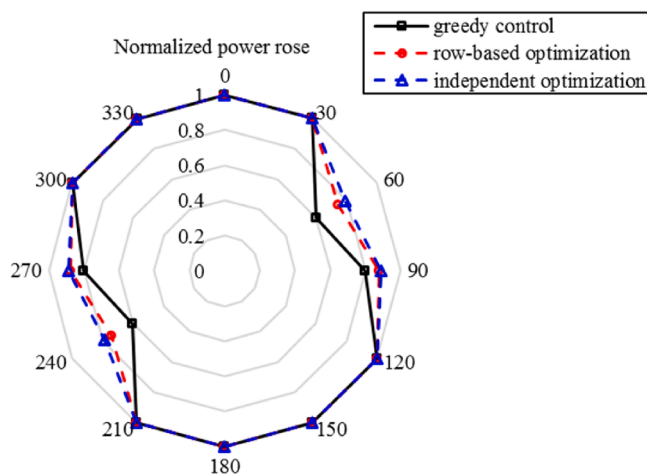


Fig. 26. Power rose diagram for staggered layout under uniform wind direction.

becomes more remarkable at the wind sectors 240° and 60° than at 270° and 90° in terms of the absolute power gain.

To explore the mechanism behind the above discrepancies between the wind directions 270° and 240°, the optimized yaw angles under wind direction 240° and the corresponding contours of wake velocity and turbulence intensity are extracted for comparisons, as illustrated in

Figs. 27, 28, and 29. As for the row-based control scheme, only the first turbine row have obvious yaw behaviors, while the yaw angle of the other turbine rows can be approximately negligible. However, a different wake steering pattern displays under the independent cooperative control scheme, where apart from the yaw misalignment of the first turbine row, the turbines sited in the margins of the subsequent rows still need to yaw to deflect the wake away from the downstream turbines. Furthermore, the turbines under the independent cooperative control scheme yaw to a more degree than the row-based one.

The hub-height wake velocity and turbulence intensity provides a more in-depth explanation for the above phenomena, as revealed in Figs. 28 and 29. Obviously, more turbines are under the full-wake effect imposed by the upstream turbines under wind direction 240° than 270°, among which some even bear the wake velocity deficit coming from the upstream consecutive three turbines. This explains why the most significant power loss appears at the wind sector 240° rather than 270°, and the yaw control strategy can create more prominent power enhancement under such circumstances. Comparing the wake velocity and turbulence intensity distributions under the row-based and independent cooperative control schemes, a more valid circumventing of the wake interference can be achieved under the independent cooperative control scheme, especially for the turbines in the last row. At the same time, the deviation in the wake structure pattern between the two control schemes also accumulates along the turbine row. As seen in Figs. 28 and 29, the unified unyawed control in the 2nd turbine row under the row-based cooperative control scheme obviously disturbs the incipient flow in front of the downstream turbines, incurring a sharper

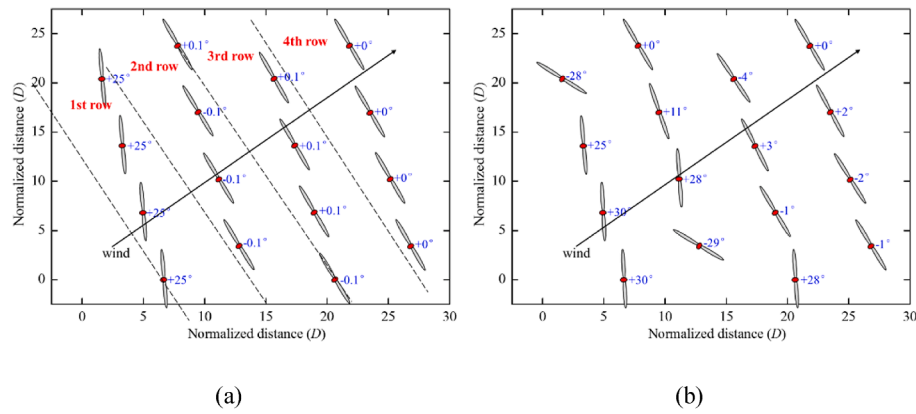


Fig. 27. Optimized yaw angles for staggered layout under wind direction 240°: (a) row-based control scheme; (b) independent control scheme.

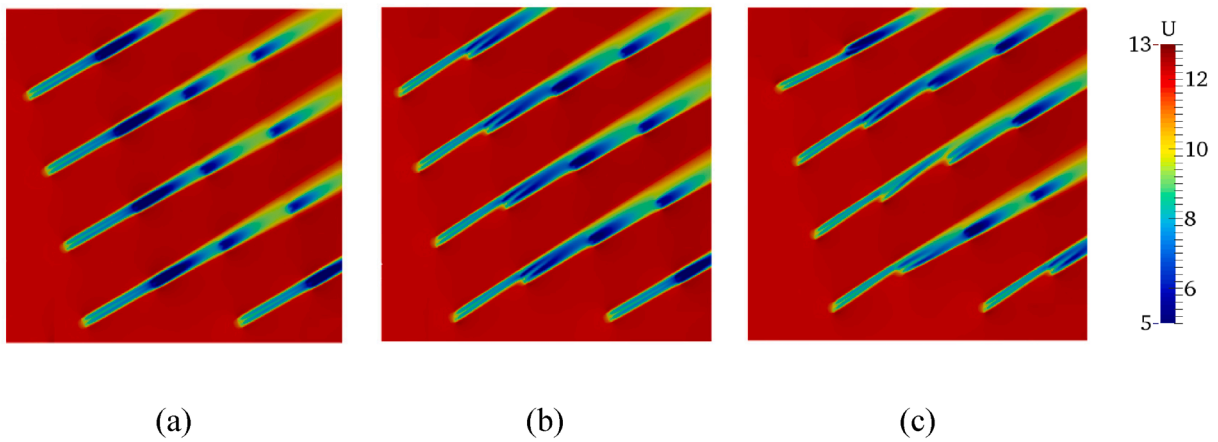


Fig. 28. Contours of velocity for staggered layout under wind direction 240°: (a) greedy control; (b) row-based control optimization; (c) independent control optimization.

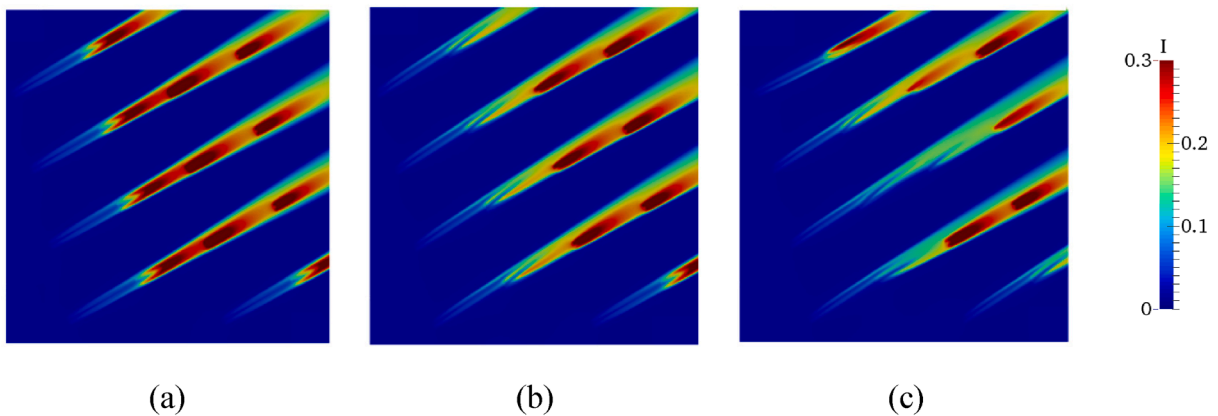


Fig. 29. Contours of turbulence intensity for staggered layout under wind direction 240°: (a) greedy control; (b) row-based control optimization; (c) independent control optimization.

fall in the inflow velocity in contrast with the one under the independent cooperative control scheme.

### 5.2.3. Wind rose

The measured wind rose in Fig. 12(b) is also applied to the staggered layout to analyze the performance of the row-based and independent optimizations in diversified wind farm layouts, as shown in Fig. 30. On the one hand, the power production without considering the yaw control

is only affected by the wind direction, which shows a symmetric pattern due to the regularity of the staggered layout. On the other hand, owing to the combined effects of wind direction and speed, the symmetry of the power rose diagram under the cooperative yaw control disappears, and there appear to be more major power improvements under wind directions 270° and 240° than their counterparts 90° and 60°. It is also interesting to note that under the wind direction 60°, the wake steering strategy almost brings no benefit to the power production, even though

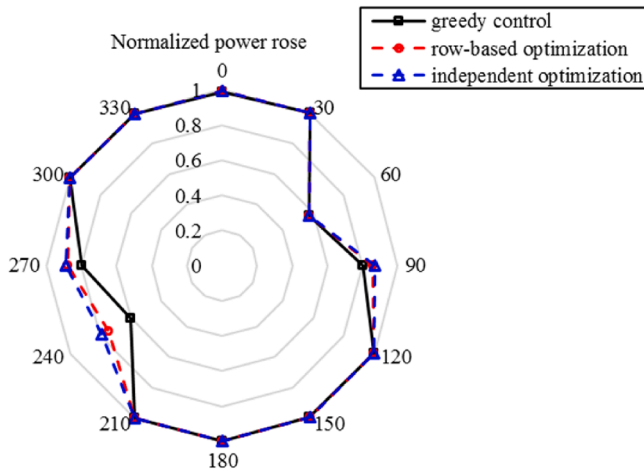


Fig. 30. Power rose diagram for staggered layout under wind rose.

the wind farm suffers from tremendous power loss. The above phenomenon can attribute to the limit on the validity of the yaw control due to the constraint of the minimum operational wind speed, especially under low wind velocity.

5.2.4. Effect of wind direction distribution in the staggered layout

Overall comparisons of the effectiveness of the two cooperative control schemes considering three wind direction distributions for the staggered layout are offered in Table 3. Note that AEP serves as the index of the power output for the uniform wind distribution and wind rose. As for the power gain directly brought by the cooperative control strategy, a drastic reduction of the power increase appears under the single wind direction compared with the aligned layout, whereas there is just a slight drop under the uniform wind direction and wind rose. When it comes to the applicability of the row-based cooperative control scheme to different wind direction distributions, the staggered layout exacerbates the deviation of its optimization result from the one based on the independent control in contrast with the aligned layout. Furthermore, the divergence of the wind direction and speed in the uniform wind direction and wind rose can widen the gap between the two optimization results compared with the single wind direction; meanwhile, the layout-induced difference in this deviation degree also rises.

5.3. Effect of layout configuration under different wind direction distributions

The impacts of the layout on the feasibility of the row-based cooperative control scheme under different wind direction distributions are summarized in Tables 4, 5, and 6, respectively. From Table 4, under the single wind direction, it can be observed that the two cooperative control schemes impose almost the same degree of impact on the difference in the power gain between the two layouts. However, the row-based control scheme can almost bring the same optimization effect as the independent one for the aligned layout, whereas it considerably falls behind the independent one for the staggered layout. From Table 5, under the uniform wind direction, the disparity of power gain between the two layouts brought by the row-based control scheme appears more

Table 3 Comparison of two control schemes for staggered layout under three wind direction distributions.

Control scheme	Single	Uniform distribution	Wind rose
Row-based	9.4%	4.0%	3.4%
Independent	11.0%	5.1%	4.3%
Difference	17.02%	27.50%	26.47%

Table 4 Comparison of two layouts for single wind direction under two control schemes.

Layout configuration	Row-based control scheme	Independent control scheme	Difference
Aligned layout	30.0%	30.4%	1.33%
Staggered layout	9.4%	11.0%	17.02%
Difference	-68.67%	-63.82%	

Table 5 Comparison of two layouts for uniform wind direction under two control schemes.

Layout configuration	Row-based control scheme	Independent control scheme	Difference
Aligned layout	4.6%	4.9%	6.52%
Staggered layout	4.0%	5.1%	27.5%
Difference	-13.04%	4.08%	

Table 6 Comparison of two layouts for wind rose under two control schemes.

Layout configuration	Row-based control scheme	Independent control scheme	Difference
Aligned layout	4.3%	4.7%	9.30%
Staggered layout	3.4%	4.3%	26.47%
Difference	-20.93%	-8.51%	

marked than the one by the independent control scheme. In addition, the uniform wind direction broadens the gap between the two control schemes for both layouts, where the deviation in the staggered layout still stands ahead of the one in the aligned layout by large. Regarding the comparisons under the wind rose in Table 6, the row-based control scheme can also incur a more noticeable discrepancy of power improvements between two layouts than the independent control scheme. Moreover, although the wind rose increases the gap between the two control schemes in the aligned layout to some degree but causes minor effects on the one in the staggered layout, the advantage of the independent control scheme over the row-based one is still pronounced in the staggered layout, but less distinct in the aligned layout. To sum up, on the one hand, with the divergence of the wind distribution, the difference in the power enhancement between the aligned and staggered layouts resulting from the row-based control scheme becomes more marked than the one induced by the independent control scheme. On the other hand, the row-based control scheme is more applicable to the aligned layout than the staggered layout owing to the diversification of the wake pattern and the cut of the inter-column spacing between the consecutive turbine rows.

5.4. Extension of row-based control scheme to larger wind farm

To further assess the performance of the row-based cooperative control scheme in larger wind farms compared with the independent one, a 49-turbine wind farm scaling up from the aligned layout in Fig. 11 is selected, as shown in Fig. 31. The power rose diagram under wind rose (Fig. 32) compares power production in each wind sector between the row-based and independent control schemes. Similarly, the distribution of power rose under greedy control displays a symmetric distribution, whereas cooperative controls bring asymmetric power improvements. However, as for the benefit comparison between the row-based and independent control schemes, slighter discrepancies can be observed at wind sectors 90° and 240° compared with the result of the 16-turbine wind farm in Fig. 22. Table 7 further lists the quantitative comparisons of the overall power enhancement between two control schemes for the 16-turbine and 49-turbine wind farms, respectively. Although the power gain induced by the cooperative control strategy experiences a

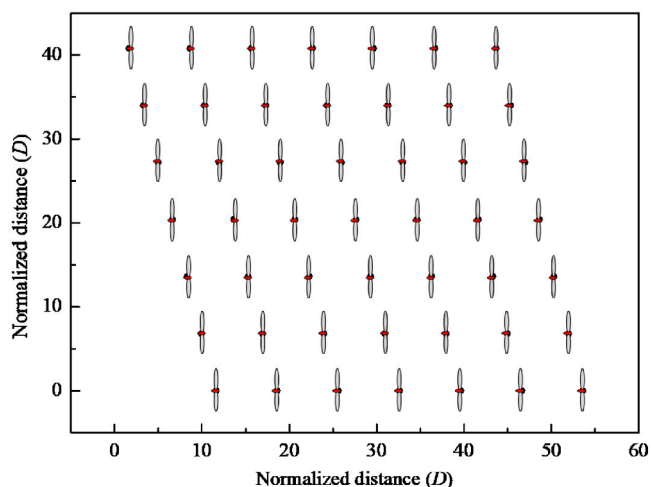


Fig. 31. Larger wind farm with seven by seven aligned layout.

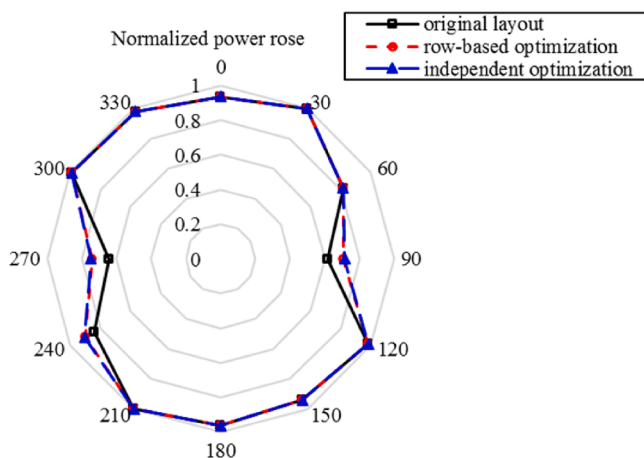


Fig. 32. Power rose diagram under wind rose for larger wind farm.

downfall with the increase of the wind farm scale, the advantage of the row-based control scheme in an aligned layout is enhanced, seeing a slighter power sacrifice of the row-based control scheme in contrast with the independent one. The above extension study justifies the excellent application potential of the row-based control scheme in larger wind farms with regular layouts.

### 6. Conclusions

This study presents a novel double-layer ML framework comprising an ANN yawed wake model and a Bayesian ML algorithm for the real-time cooperative wind farm control with high accuracy and efficiency. The ANN yawed wake model in the 1st layer establishes a black box bridging the inputs (inflow and yaw conditions) and outputs (wake fields) and can predict the total power production of the wind farm combined with empirical superposition models. The Bayesian ML framework can locate the optimally coordinated control actions with the power prediction data fed by the 1st layer. Given the control on the

Table 7  
Comparison of two control schemes for 16-turbine and 49-turbine wind farms.

Control scheme	16-turbine wind farm	49-turbine wind farm
Row-based	4.3%	2.7%
Independent	4.7%	2.9%
Difference	9.30%	7.41%

iteration number with the scale-up of the wind farm, this study further puts forward a new row-based control scheme to improve the optimization rate by reasonably reducing the optimization parameters. A 16-turbine wind farm is selected as the case study to evaluate its performance in optimization efficiency compared with the general independent control scheme. Then the influence of wind distribution and layout configuration on its feasibility is also profoundly explored. Meanwhile, the row-based control scheme is further assessed in a larger 49-turbine wind farm. Based on the sensitivity mentioned above, recommendations on the suitability of the row-based control scheme to engineering practice are made, with different wind distributions and layout designs considered. Several main results are summarized:

- (a) The proposed ANN yawed wake model performs favorably in standalone and multiple wake modelings, thus creating an accurate and efficient wind farm power prediction, which lends great credence to its application to the cooperative yaw control of the large-scale wind farm.
- (b) Based on the decent optimization efficiency of the double-layer ML framework, the row-based control scheme can further improve the convergence rate of the Bayesian ML algorithm remarkably at the expense of a slight decrease in optimal power production. For the case of a 16-turbine wind farm with an aligned layout configuration, an upgrade of the optimization rate by six times is accomplished at the expense of only a 0.3% power loss.
- (c) The divergence of the wind distribution for the uniform wind direction and wind rose can dwindle the power gain of the wake steering strategy and also weaken the superiority of the row-based cooperative control scheme over the general independent one, in contrast with the single wind direction.
- (d) The row-based cooperative control scheme is more applicable to the aligned layout than the staggered layout owing to the diversification of the wake pattern and the cut of the inter-column spacing between the consecutive turbine rows. Meanwhile, with the divergence of the wind distribution, the difference in the power enhancement between the aligned and staggered layout resulting from the row-based control scheme becomes more marked than the one induced by the independent control scheme. In addition, the advantage of the row-based control scheme in an aligned layout is enhanced with the increase of wind farm scale.

Ongoing research on validating the feasibility of the row-based control scheme in the engineering practice considering more complex wind distribution and irregular layout is underway. Considering the possible limitation of the row-based control scheme applied to the regular layout, future research on the cooperative control under the irregular layout is also under investigation, focusing on the more advanced two-stage cooperative control scheme, involving the optimal wind farm partition method. A more comprehensive optimization target with simultaneous considerations of the power and loading will also be further investigated.

### CRedit authorship contribution statement

**Shanghai Yang:** Methodology, Investigation, Software, Validation, Data curation, Writing – original draft. **Kun Yang:** Investigation, Visualization. **Xiaowei Deng:** Conceptualization, Supervision, Writing – review & editing. **Jun Yang:** Supervision, Funding acquisition, Writing – review & editing.

### Declaration of Competing Interest

The authors declare that they have no known competing financial interests or personal relationships that could have appeared to influence the work reported in this paper.

## Data availability

No data was used for the research described in the article.

## Acknowledgment

This work is generously supported by the Research Grants Council via RGC/CRF (C7038-20GF) and RGC/GRF (17204122), Shenzhen Science and Technology Innovation Committee via Fundamental Research General Program (2021302011), and National Natural Science Foundation of China via General Program (Project No. 51878586). The computations were mainly performed using research computing facilities offered by Information Technology Services, the University of Hong Kong.

## References:

- [1] M. F. Howland, S. K. Lele, and J. O. Dabiri, "Wind farm power optimization through wake steering," *Proceedings of the National Academy of Sciences*, vol. 116, no. 29, pp. 14495-14500, 2019.
- [2] Yang S, Deng X, Zhang M, Xu Y. Effect of wave spectral variability on the dynamic response of offshore wind turbine considering soil-pile-structure interaction. *Ocean Eng* 2023;267:113222.
- [3] Yang S, Deng X, Yang J. Modeling of soil-pile-structure interaction for dynamic response of standalone wind turbines. *Renew Energy* 2022;186:394-410.
- [4] Burton T, Jenkins N, Sharpe D, Bossanyi E. *Wind energy handbook*. John Wiley & Sons; 2011.
- [5] Park J, Law KH. Cooperative wind turbine control for maximizing wind farm power using sequential convex programming. *Energy Conver Manage* 2015;101:295-316.
- [6] Jensen NO. A note on wind generator interaction. *Citeseer*; 1983.
- [7] Frandsen S. On the wind speed reduction in the center of large clusters of wind turbines. *J Wind Eng Ind Aerodyn* 1992;39(1-3):251-65.
- [8] Bastankhah M, Porté-Agel F. A new analytical model for wind-turbine wakes. *Renew Energy* 2014;70:116-23.
- [9] Sun H, Gao X, Yang H. Validations of three-dimensional wake models with the wind field measurements in complex terrain. *Energy* 2019;189:116213.
- [10] Dou B, Guala M, Lei L, Zeng P. Wake model for horizontal-axis wind and hydrokinetic turbines in yawed conditions. *Appl Energy* 2019;242:1383-95.
- [11] Ishihara T, Qian G-W. A new Gaussian-based analytical wake model for wind turbines considering ambient turbulence intensities and thrust coefficient effects. *J Wind Eng Ind Aerodyn* 2018;177:275-92.
- [12] Bastankhah M, Porté-Agel F. Experimental and theoretical study of wind turbine wakes in yawed conditions. *J Fluid Mech* 2016;806:506-41.
- [13] Shapiro CR, Gayme DF, Meneveau C. Modelling yawed wind turbine wakes: a lifting line approach. *J Fluid Mech* 2018;841.
- [14] Lopez D, Kuo J, Li N. A novel wake model for yawed wind turbines. *Energy* 2019; 178:158-67.
- [15] Fleming PA, Ning A, Gebraed PM, Dykes K. Wind plant system engineering through optimization of layout and yaw control. *Wind Energy* 2016;19(2):329-44.
- [16] van Dijk MT, van Wingerden J-W, Ashuri T, Li Y. Wind farm multi-objective wake redirection for optimizing power production and loads. *Energy* 2017;121:561-9.
- [17] Dou B, Qu T, Lei L, Zeng P. Optimization of wind turbine yaw angles in a wind farm using a three-dimensional yawed wake model. *Energy* 2020;209:118415.
- [18] Qian G-W, Ishihara T. A new analytical wake model for yawed wind turbines. *Energies* 2018;11(3):665.
- [19] Ti Z, Deng XW, Yang H. Wake modeling of wind turbines using machine learning. *Appl Energy* 2020;257:114025.
- [20] Ti Z, Deng XW, Zhang M. Artificial Neural Networks based wake model for power prediction of wind farm. *Renew Energy* 2021;172:618-31.
- [21] Yang S, Deng X, Ti Z, Yan B, Yang Q. Cooperative yaw control of wind farm using a double-layer machine learning framework. *Renew Energy* 2022;193:519-37.
- [22] Mosetti G, Poloni C, Diviacco B. Optimization of wind turbine positioning in large windfarms by means of a genetic algorithm. *J Wind Eng Ind Aerodyn* 1994;51(1): 105-16.
- [23] Parada L, Herrera C, Flores P, Parada V. Wind farm layout optimization using a Gaussian-based wake model. *Renew Energy* 2017;107:531-41.
- [24] Chen Y, Li H, Jin K, Song Q. Wind farm layout optimization using genetic algorithm with different hub height wind turbines. *Energy Conver Manage* 2013;70:56-65.
- [25] Chowdhury S, Zhang J, Messac A, Castillo L. Unrestricted wind farm layout optimization (UWFO): Investigating key factors influencing the maximum power generation. *Renew Energy* 2012;38(1):16-30.
- [26] Yang Q, Li H, Li T, Zhou X. Wind farm layout optimization for leveled cost of energy minimization with combined analytical wake model and hybrid optimization strategy. *Energy Conver Manage* 2021;248:114778.
- [27] Li B, et al. Study of three wake control strategies for power maximization of offshore wind farms with different layouts. *Energy Conver Manage* 2022;268: 116059.
- [28] Andersson LE, Anaya-Lara O, Tande JO, Merz KO, Imsland L. Wind farm control-Part I: A review on control system concepts and structures. *IET Renew Power Gener* 2021;15(10):2085-108.
- [29] Gu B, Meng H, Ge M, Zhang H, Liu X. Cooperative multiagent optimization method for wind farm power delivery maximization. *Energy* 2021;233:121076.
- [30] Rak BP, Pereira RS. Impact of the wake deficit model on wind farm yield: A study of yaw-based control optimization. *J Wind Eng Ind Aerodyn* 2022;220:104827.
- [31] Rott A, Doekemeijer B, Seifert JK, van Wingerden J-W, Kühn M. Robust active wake control in consideration of wind direction variability and uncertainty. *Wind energy science* 2018;3(2):869-82.
- [32] Park J, Law KH. A data-driven, cooperative wind farm control to maximize the total power production. *Appl Energy* 2016;165:151-65.
- [33] Park J, Law KH. Bayesian ascent: A data-driven optimization scheme for real-time control with application to wind farm power maximization. *IEEE Trans Control Syst Technol* 2016;24(5):1655-68.
- [34] Gionfra N, Sandou G, Siguerdidjane H, Faille D, Loevenbruck P. Wind farm distributed PSO-based control for constrained power generation maximization. *Renew Energy* 2019;133:103-17.
- [35] Shu T, Song D, Joo YH. Decentralised optimisation for large offshore wind farms using a sparsified wake directed graph. *Appl Energy* 2022;306:117986.
- [36] Siniscalchi-Minna S, Bianchi FD, Ocampo-Martinez C, Domínguez-García JL, De Schutter B. A non-centralized predictive control strategy for wind farm active power control: A wake-based partitioning approach. *Renew Energy* 2020;150: 656-69.
- [37] Annoni J, et al. Wind direction estimation using SCADA data with consensus-based optimization. *Wind Energy Science* 2019;4(2):355-68.
- [38] Greenshields CJ. *OpenFOAM user guide*. OpenFOAM Foundation Ltd, version 2015;3(1):47.
- [39] Yegnanarayana B. *Artificial neural networks*. PHI Learning Pvt Ltd 2009.
- [40] Gulli A, Pal S. *Deep learning with Keras*. Packt Publishing Ltd 2017.
- [41] J. Y. Kuo, D. A. Romero, and C. H. Amon, "A novel wake interaction model for wind farm layout optimization," in *ASME International Mechanical Engineering Congress and Exposition*, 2014, vol. 46521: American Society of Mechanical Engineers, p. V06BT07A074.
- [42] N. Trolborg, "Actuator line modeling of wind turbine wakes," 2009.
- [43] Mockus J, Tiesis V, Zilinskas A. The application of Bayesian methods for seeking the extremum. *Towards global optimization* 1978;2(117-129):2.
- [44] Wu Y-T, Porté-Agel F. Atmospheric turbulence effects on wind-turbine wakes: An LES study. *Energies* 2012;5(12):5340-62.
- [45] Wu Y-T, Porté-Agel F. Modeling turbine wakes and power losses within a wind farm using LES: An application to the Horns Rev offshore wind farm. *Renew Energy* 2015;75:945-55.
- [46] Porté-Agel F, Wu Y-T, Chen C-H. A numerical study of the effects of wind direction on turbine wakes and power losses in a large wind farm. *Energies* 2013;6(10): 5297-313.